Journal Pre-proof

Synthesis and *in vitro* evaluation of novel spiroketopyrazoles as acetyl-CoA carboxylase inhibitors and potential antitumor agents

Tonghui Huang, Xin Wu, Shirong Yan, Tianya Liu, Xiaoxing Yin

PII: S0223-5234(20)31008-4

DOI: https://doi.org/10.1016/j.ejmech.2020.113036

Reference: EJMECH 113036

To appear in: *European Journal of Medicinal Chemistry*

Received Date: 25 September 2020

Revised Date: 6 November 2020

Accepted Date: 14 November 2020

Please cite this article as: T. Huang, X. Wu, S. Yan, T. Liu, X. Yin, Synthesis and *in vitro* evaluation of novel spiroketopyrazoles as acetyl-CoA carboxylase inhibitors and potential antitumor agents, *European Journal of Medicinal Chemistry*, https://doi.org/10.1016/j.ejmech.2020.113036.

This is a PDF file of an article that has undergone enhancements after acceptance, such as the addition of a cover page and metadata, and formatting for readability, but it is not yet the definitive version of record. This version will undergo additional copyediting, typesetting and review before it is published in its final form, but we are providing this version to give early visibility of the article. Please note that, during the production process, errors may be discovered which could affect the content, and all legal disclaimers that apply to the journal pertain.

© 2020 Elsevier Masson SAS. All rights reserved.

Graphical Abstract

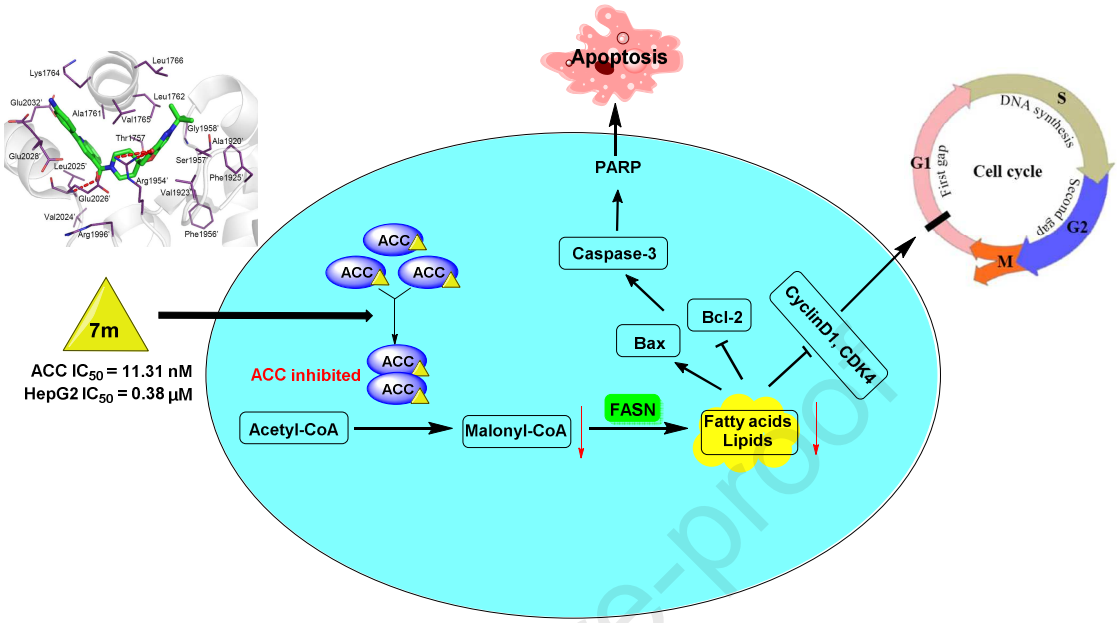

Compound **7m** exhibited significant anti-proliferative activity in HepG2 cells.

Journal Pre-proof

Synthesis and *in vitro* evaluation of novel spiroketopyrazoles as acetyl-CoA carboxylase inhibitors and potential antitumor agents

Tonghui Huang[a, b, 1, *], Xin Wu[a, 1], Shirong Yan[a], Tianya Liu[c], Xiaoxing Yin[a, *]

[a] *Jiangsu Key Laboratory of New Drug Research and Clinical Pharmacy, Xuzhou Medical University, 221004 Xuzhou, Jiangsu, China.*

[b] *Xuzhou Medical University Science Park, 221000, Xuzhou, Jiangsu, People's Republic of China.*

[c] *Department of Pharmacy, The Affiliated Hospital of Xuzhou Medical University, 221002 Xuzhou, Jiangsu, China.*

Graphical Abstract

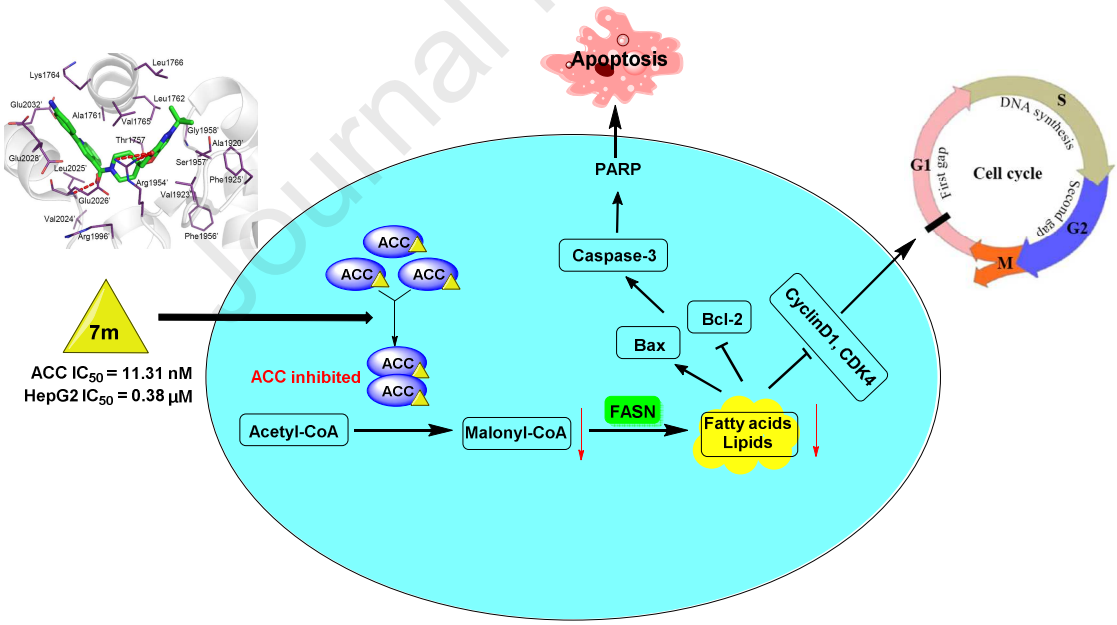

Compound **7m** exhibited significant anti-proliferative activity in HepG2 cells.

[1] These two authors contributed equally to this work.

* Corresponding authors: Xiaoxing Yin, yinxx@xzhmu.edu.cn; Tonghui Huang, tonghhuang@xzhmu.edu.cn.

Abstract

Acetyl-CoA carboxylase (ACC) is a rate-limiting enzyme in *de novo* fatty acid synthesis, which plays a critical role in the growth and survival of cancer cells. In this study, a series of spiroketopyrazole derivatives bearing quinoline moieties were synthesized, and *in vitro* anticancer activities of these compounds as ACC inhibitors were evaluated. The biological evaluation showed that compound **7j** exhibited the strongest enzyme inhibitory activity (IC_{50} = 1.29 nM), while compound **7m** displayed the most potent anti-proliferative activity against A549, HepG2, and MDA-MB-231 cells with corresponding IC_{50} values of 0.55, 0.38, and 1.65 μM, respectively. The preliminary pharmacological studies confirmed that compound **7m** reduced the intracellular malonyl-CoA and TG levels in a dose-dependent manner. Moreover, it could down-regulate cyclin D1 and CDK4 to disturb the cell cycle and up-regulate Bax, caspase-3, and PARP along with the suppression of Bcl-2 to induce apoptosis. Notably, the combination of **7m** with doxorubicin synergistically decreased the HepG2 cell viability. These results indicated that compound **7m** as a single agent, or in combination with other antitumor drugs, might be a promising therapeutic agent for the treatment of hepatocellular carcinoma.

Keywords: acetyl-CoA carboxylase; anticancer; apoptosis; drug combination.

Journal Pre-proof

Journal Pre-proof

1. Introduction

Malignant cells usually have an extraordinary demand for cellular building blocks, such as proteins, nucleotides, and lipids, to support continuous proliferation [1, 2]. Therefore, they tend to reprogram their metabolic pathways, which have been denoted to be the emerging hallmark of cancer [3-5]. One of the most prominent features of metabolic reprogramming is the elevated rate of *de novo* fatty acid synthesis (FASyn) [6]. Unlike normal cells that primarily uptake energy-providing lipids from the diet, malignant cells principally use lipids coming from FASyn [7, 8]. Moreover, numerous cancers, including those of the lung, liver, breast, prostate, and colon, have demonstrated an enhancement in the rate of FASyn, and the modulation of the lipogenic enzymes involved in the FASyn process has shown significant inhibition in cell division and proliferation [9-11].

Acetyl-CoA carboxylase (ACC) is a crucial enzyme in fatty acid metabolism, which catalyzes the ATP-dependent carboxylation of acetyl-CoA to produce malonyl-CoA [12]. There are two well-characterized isoforms of mammalian ACC, namely ACC1 and ACC2, with disparate subcellular distributions and physiological significance. ACC1 is a cytosolic isoform that primarily responsible for FASyn, whereas ACC2, an isoform embedded in the outer membrane of mitochondria, is mainly in charge of the fatty acid oxidation (FAOxn) [13]. Due to the importance of ACC in fatty acid metabolism, it has emerged as an attractive target for the treatment of various diseases, including type 2 diabetes mellitus (T2DM), bacterial infections, and most recently, cancer [14-16]. The research on cancer initiation and progression mainly focuses on the ACC1 isoform due to the up-regulation of ACC1 mRNA involved in most of the cancers [17-21]. In addition, the ACC1 silencing or deletion was documented to significantly decrease FASyn, induce cell cycle arrest and apoptosis, and ultimately lead to tumor cell death, while supplementation with

exogenous palmitate could completely rescue this effect [22, 23].

Although a variety of ACC inhibitors have been identified, only a few were found to exhibit antitumor activities (Fig. 1) [24-30]. Compound **PF-1** (ACC1 IC_{50} = 17 nM, Fig. 2) is a potent and orally bioavailable ACC inhibitor that was originally designed by Pfizer for the treatment of T2DM [31], and in 2018, its derivative **PF-2** was found to demonstrate significant cytotoxicity toward A549 and H1975 cells [29]. Based on this research, the anti-proliferative activity of **PF-1** was assessed (Table 2). However, the inhibitory effect of **PF-1** on cancer cells was not in par with its strong enzyme activity, which was speculated to be attributed to the low lipophilicity and passive permeability of this compound. Furthermore, the co-crystal structure of **PF-1** bound to the carboxyl transferase (CT) domain of humanized yeast ACC revealed that the pyrazolopyranone moiety was located in a hydrophobic groove and the structural rigidity of the spirocycle was essential for the binding [32]. Therefore, this study focused on seeking a scaffold that would provide an optimal fit in the binding pocket, while improving the overall lipophilicity.

Compound **AZ-1** is a moderate ACC inhibitor, as identified from the high throughput screening (IC_{50} = 3.6 μM, Fig. 2) [33]. In contrast to the 5-carboxyindazole group of **PF-1**, the quinoline carboxylic acid group of **AZ-1** is more lipophilic and can be conveniently optimized through the established synthetic pathways [34]. Taking these advantages into account, a spiroketopyrazole scaffold possessing quinoline moieties was designed, and various aryl or alkoxy substituents were introduced to occupy the hydrophobic pocket (Fig. 2). It was proposed that the hybridization could enhance the ligand affinity and passive permeability, ultimately leading to an increase in ACC inhibitory as well as antitumor activities.

Herein, a series of spiroketopyrazole derivatives bearing quinoline moieties were designed and synthesized to act as novel ACC inhibitors. The synthesized compounds

were evaluated for their biological activity toward the ACC1 enzyme and three different cancer cell lines. Moreover, the underlying receptor-ligand interactions and preliminary pharmacological studies were performed on representative compounds to elucidate the mechanistic action of spiroketopyrazoles.

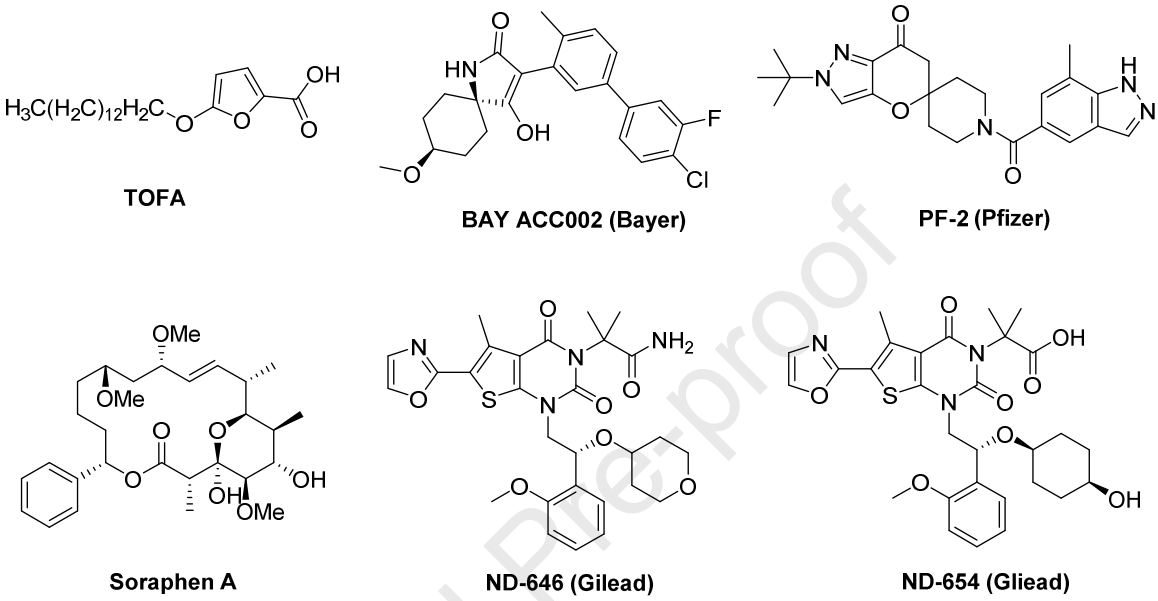

Fig. 1 Representative of ACC inhibitors with antitumor activity.

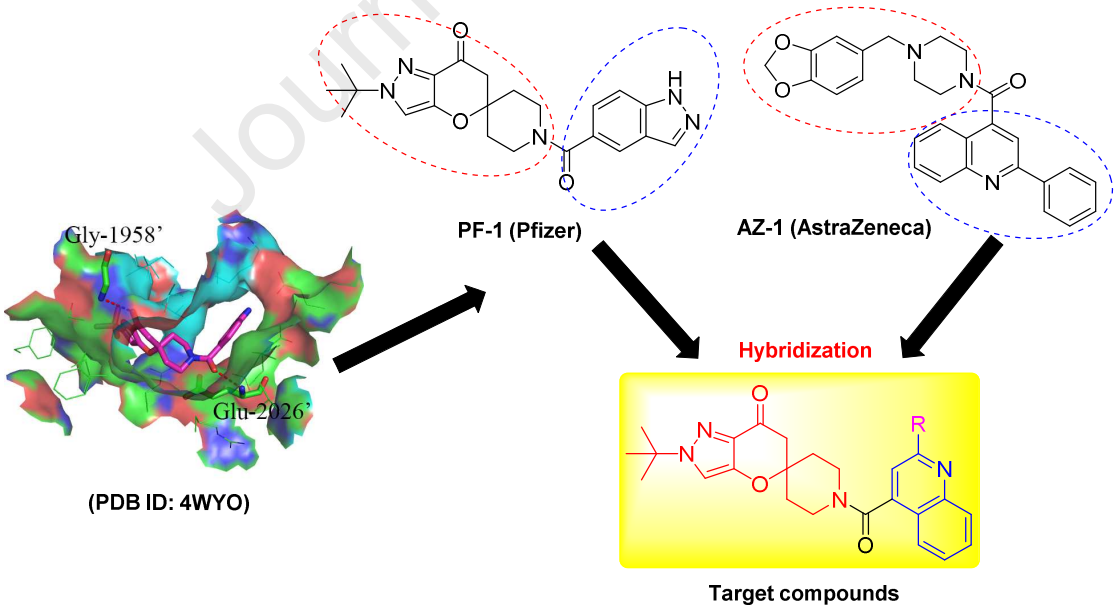

Fig. 2 The design strategy of spiroketopyrazoles bearing quinoline moieties as ACC inhibitors.

2. Results and discussion

2.1 Chemisry

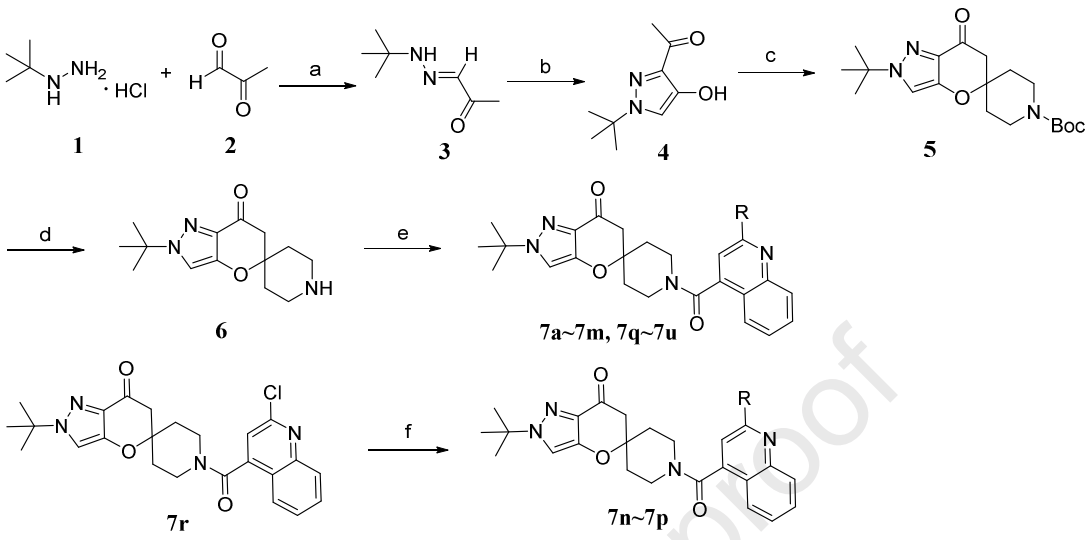

7a: R = phenyl
7b: R = 4-methyl phenyl
7c: R = 2-methyl phenyl
7d: R = 4-chloro phenyl
7e: R = 2-chloro phenyl
7f: R = 4-fluoro phenyl
7g: R = 4-bromo phenyl
7h: R = 4-methoxyphenyl
7i: R = 3,4-dimethoxy phenyl
7j: R = 4-amino phenyl
7k: R = 4-dimethylamino phenyl
7l: R = pyridin-2-yl
7m: R = pyridin-4-yl
7n: R = piperazin-1-yl
7o: R = 4-methylpiperazin-1-yl
7p: R = 4-morpholino
7q: R = methyl
7r: R = chloro
7s: R = methoxyl
7t: R = ethyoxyl
7u: R = isopropoxyl

Scheme 1. Synthesis of target compounds **7a~7u**. Reagents and conditions: (a) H_2O, r.t., 2 h, 85%; (b) glyoxal (40 wt.% solution in H_2O), H_2O, reflux, 5 h, 80%; (c) THF, MeOH, N-(tert-Butoxycarbonyl)-4-piperidone, r.t. to reflux, 24 h, 60%; (d) TFA, CH_2Cl_2, r.t., 2 h, 95%; (e) HATU, triethylamine, DMF, r.t., 12 h, 45-75%; (f) amines, reflux, 2 h, 30-60%.

The synthetic route of the spiroketopyrazole derivatives **7a~7u** is shown in Scheme 1. To brief, the intermediate **3** was readily generated by the nucleophilic addition of the commercially available compounds **1** and **2**. Later, the hydrazone **3** was reacted with glyoxal in an aqueous solution to provide the intermediate **4**, which was finally converted into the key intermediate **5** under a base-catalyzed spiro-cyclization reaction in the presence of N-(*tert*-Butoxycarbonyl)-4-piperidone [31]. The Boc-protecting group was removed using trifluoroacetic acid. The final compounds **7a~7m** and **7q~7u** were conveniently prepared by the condensation of intermediate **6** with different quinoline-4-carboxylic acid derivatives. Furthermore,

the nucleophilic substitution reaction of compound **7r** with nitrogen heterocycles offered the desired compounds **7n~7p** in a straightforward manner.

2.2 In vitro ACC inhibitory activity

To evaluate the enzymatic inhibitory activity of the target compounds, a well-established luminescent ADP detection assay against ACC1 enzyme was performed. Firsocostat (formerly ND-630), an ACC inhibitor under Phase II trial, was selected as the reference compound along with **PF-1** [35, 36]. As shown in Table 1, the initial screening results of the spiroketopyrazole derivatives were generally gratifying. All the compounds showed inhibition rates (IR) of greater than 90% under a concentration of 5 μM, and when the concentration was reduced to 0.1 μM, most aryl or pyridine derivatives also displayed significant inhibition toward ACC1 (IR > 80%). However, the inhibitory effect decreased remarkably for the compounds with non-aromatic substituents (**7n~7u**, IR: 36.66% ~ 67.97%), which highlighted the importance of aromaticity in ACC inhibition. Besides, the potency of compounds **7c** and **7e** were weaker than the other substituted-phenyl derivatives, indicating that the *o*-substitution on the phenyl was not conducive to the protein-small molecule interactions.

Encouraged by the above results, the IC_{50} values of the synthesized compounds were subsequently calculated to further explore the structure-activity relationship (SAR). A total of eleven compounds with stronger potencies in comparison with **PF-1** were identified, which were unsurprisingly substituted by aromatic groups. Among them, the pyridine substituted compounds **7l** and **7m** were found to exhibit similar inhibitory activities as that of **PF-1**, with the IC_{50} values of 13.84 nM and 11.31 nM, respectively. In contrast, the IC_{50} value of the phenyl-substituted compound **7a** (IC_{50} = 6.00 nM) was twice lower than **PF-1**, indicating the unique advantage of phenyl in inhibiting the enzymatic activity. Moreover, on substituting the phenyl with

electron-neutral (4-CH_3) or electron-rich (4-OCH_3, 3,4-OCH_3, 4-NH_2, 4-$N(CH_3)_2$) groups, the IC_{50} values of the corresponding compounds (**7b**, **7h~7k**) were further decreased, with the *p*-aminophenyl substituted compound **7j** exhibiting the best ACC inhibitory activity (IC_{50} = 1.29 nM).

Table 1. The ACC1 inhibitory activity and calculated physicochemical properties of **7a~7u**.

Compounds	IR (%) [a]		IC_{50} (nM) [a]	cLogP [b]	LLE [c]
	5 μM	0.1 μM			
7a	100.69	90.54	6.00	3.99	4.23
7b	101.35	93.76	2.22	4.49	4.16
7c	95.53	41.84	> 100	4.19	ND
7d	103.89	93.22	6.09	4.71	3.51
7e	94.39	43.61	> 100	4.46	ND
7f	100.46	87.26	9.40	4.14	3.89
7g	102.23	93.25	5.67	4.86	3.39
7h	100.55	94.76	3.18	4.01	4.49
7i	101.95	95.58	3.57	3.72	4.73
7j	101.46	94.14	1.29	2.95	5.94
7k	99.63	96.39	2.72	4.27	4.29
7l	103.07	84.04	13.84	2.79	5.07
7m	100.31	86.25	11.31	2.58	5.37
7n	97.56	59.62	> 20	1.90	ND
7o	97.43	52.77	> 20	2.46	ND
7p	97.67	56.89	> 20	1.88	ND
7q	93.60	55.03	> 20	2.39	ND
7r	96.74	59.08	> 20	2.64	ND
7s	93.76	36.66	> 100	2.66	ND
7t	93.88	38.40	> 100	3.19	ND
7u	99.37	67.97	> 20	3.50	ND
PF-1	101.35	82.46	17.28	1.57	6.17
ND-630	---	---	4.34	---	---

[a] The data represent the mean values of two independent experiments.

[b] cLogP values were estimated by Molsoft.

[c] LLE values were calculated according to the formula LLE = pIC_{50} – cLogP; ND: not determined.

2.3 Molecular docking

To gain insight into the binding modes of the synthesized compounds with ACC enzyme, the molecular docking studies of representative compounds (**7a**, **7b**, **7j**, and **7l**) were performed using the software Sybyl-X 2.1, with the results visualized by PyMOL [37]. The initial configuration of the binding pocket was determined based on the co-crystal structure of the ACC CT domain with **PF-1** (PDB ID: 4WYO) [32], and the docking protocol was validated by re-docking the energy-minimized **PF-1** into the theoretical binding pocket. As illustrated in Fig. 3A, the post-optimized ligand was effectively overlapped with the original ligand, and a reasonable root-mean-square deviation (RMSD) value was obtained (1.493 Å), which implied the reliability of the docking settings used in this study.

Based on the above information, the selected compounds were energy-minimized as described in the experimental section, and docked into the hydrophobic binding pocket. As expected, compounds **7a**, **7b**, and **7l** exhibited similar binding modes as that of **PF-1**. These compounds were oriented at the active site of the CT dimer interface with constant hydrogen-bonded interactions (Fig. 3B). However, the binding mode of the most potent derivative **7j** was obviously distinct from the rest. The ketone carbonyl of **7j** was closer to Arg-1954' rather than Glu-2026', and two new hydrogen bonds were observed between the ketone and Arg-1954', which partly explained its excellent ACC inhibitory activity (Fig. 3C). Notably, it is presumed from this finding that the shift in the ketone position may provide a promising option for the design of ACC inhibitors in the future.

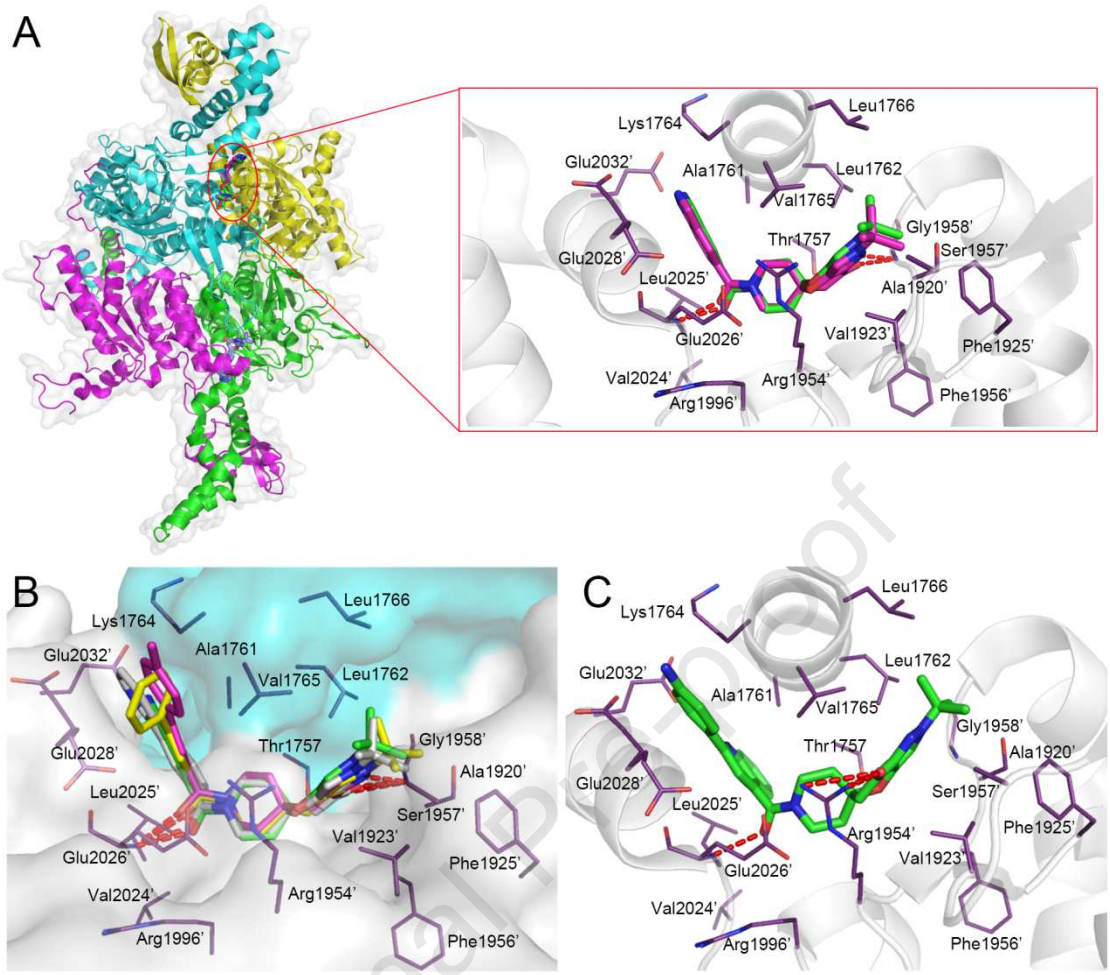

Fig. 3 Molecular docking studies for representative compounds (PDB ID: 4WYO). (A) Overlay of the original **PF-1** (green) with optimized **PF-1** (magenta). (B) Superimposition docking conformation of compounds **PF-1** (green), **7a** (yellow), **7b** (magenta), and **7l** (grayish) with ACC CT domain. Surface of the binding site is colored in cyan for the N domain and white for the C domain. (C) Docking model of compound **7j** (green) with the active site of the CT domain. All hydrogen bonds are highlighted in red dashed lines.

2.4 In vitro anticancer evaluation

To identify the potential ACC inhibitors for cancer treatment, the cytotoxicity of the synthesized compounds against A549, HepG2, and MDA-MB-231 cells was evaluated using the MTT assay. ACC1 is highly expressed in these cells, which facilitates a proper assessment of the bioactivity of ACC inhibitors [22, 27, 28]. The preliminary screening assay was performed at a fixed concentration of 10 μM, with doxorubicin (DOX) serving as the positive control (Fig. S1). Overall, the spiroketopyrazole derivatives exhibited varying degrees of cytotoxicity against the

three cancer cells. Most of them showed high activity against HepG2 cells, moderate activity against A549 cells, and low activity against MDA-MB-231 cells. Moreover, certain compounds were shown to be effective against the three cancer cell lines, in which **7m** exhibited the best inhibition on A549, HepG2, and MDA-MB-231 cells, with IR values of 79.29%, 80.13%, and 72.20%, respectively.

During the initial screening process, it was observed that the antitumor effects of the spiroketopyrazoles were not completely consistent with their ACC inhibitory activities. It was supposed to be attributed to the difference in the lipophilicity of target compounds. Therefore, the logarithm of the octanol-water partition coefficient (LogP) was predicted using the Molsoft online software [38]. Moreover, the lipophilic ligand efficiency (LLE), a metric used to evaluate the affinity of a ligand relative to its lipophilicity, was calculated by subtracting the cLogP from the negative $\log_{10}$ of the potency against ACC [39]. The IC_{50} values of spiroketopyrazoles against A549, HepG2, and MDA-MB-231 cancer cells, as well as their cLogP and LLE values, are summarized in Tables 1 and 2.

Similar to the initial screening results, the spiroketopyrazoles containing different substituent groups exhibited significantly different inhibitory effects on the cancer cells. Most of the aromatic substituted compounds (**7a**~**7k**) were found to display reasonable anti-proliferative activity toward A549 and HepG2 cell lines. However, only two compounds (**7i** and **7j**) with relatively low cLogP values exhibited marginally satisfactory performance toward the inhibition of MDA-MB-231 cells, indicating the crucial role of lipophilicity in the growth inhibition of these cells. Besides, compound **7j** was found to comply with the physicochemical profiles of oral drugs (cLogP = 2.95, LLE = 5.94) and exhibit considerable antitumor activity against the three cancer cell lines [40], with IC_{50} values of 0.97, 0.63, and 4.96 μM, respectively.

The pyridine-substituted derivatives **7l** and **7m** were potent antitumor agents for the three cancer cell lines, with **7m** exhibiting the strongest anti-proliferative effect among the synthesized compounds. The IC_{50} values of **7m** toward A549, HepG2, and MDA-MB-231 cells were 0.55, 0.38, and 1.65 μM, respectively, which were apparently superior to those of **PF-1**. Moreover, the cytotoxicity of **7m** against A549 and HepG2 cells was better than DOX, suggesting the ability of the compound to serve as a promising candidate for cancer treatment. The enhanced bioactivity for **7m** may be attributed to the reasonable balance between the enzyme activity, lipophilicity, and LLE value of the compound. On the other hand, the substitution of the compounds with non-aromatic groups (**7n**~**7u**) caused a significant decrease in the antitumor activity against A549 and HepG2 cells, which was consistent with their moderate ACC1 inhibitory effects. However, the anti-proliferative activity of these compounds toward MDA-MD-231 cells was satisfactory. This could be the result of the low lipophilicity of compounds **7n**~**7u**.

To further investigate the selectivity of the target compounds toward cancer cells, the human umbilical vein endothelial cells (HUVEC) were chosen for further testing [41]. As shown in Table 2, most of the compounds were essentially non-toxic to HUVEC, and those with strong antitumor activities (IC_{50} < 1 μM), namely **7d**, **7 g**, **7j**, and **7m**, exhibited less than 20% IR toward HUVEC, which demonstrated the good cancer cell selectivity of spiroketopyrazoles. The abnormal toxicity of **7b**, **7c**, and **7p** could be attributed to the off-target effects of these compounds.

Table 2. Anti-proliferative activity of **7a~7u** against three cancer cell lines and HUVEC [a].

Compounds	IC_{50} (μM)			Cell viability (%) of HUVEC [b]
	A549	HepG2	MDA-MB-231	
7a	1.94±0.49	2.11±0.49	>10	97.34±3.42
7b	5.30±1.16	1.44±0.34	>10	49.56±5.00
7c	1.88±0.12	>10	>10	38.62±4.31

7d	2.33±0.48	0.63±0.15	>10	87.33±3.85
7e	2.18±0.15	>10	>10	102.7±5.17
7f	5.77±0.29	2.93±0.35	>10	98.69±3.33
7g	9.30±1.31	0.82±0.12	>10	84.14±11.08
7h	3.74±0.89	2.78±0.36	>10	102.3±3.14
7i	2.03±0.47	1.56±0.32	7.13±1.00	93.67±1.37
7j	0.97±0.18	0.63±0.09	4.96±0.32	84.85±7.73
7k	1.15±0.10	1.73±0.22	>10	91.32±4.63
7l	7.72±0.93	1.50±0.09	8.10±1.23	103.7±7.46
7m	0.55±0.08	0.38±0.05	1.65±0.32	95.23±4.59
7n	>10	8.57±1.04	4.20±0.76	102.2±3.71
7o	>10	9.55±0.51	8.13±0.28	93.45±4.82
7p	>10	4.57±0.46	3.18±0.19	34.43±5.29
7q	>10	9.48±3.33	4.86±0.19	101.0±5.43
7r	7.17±0.30	4.72±0.16	9.22±1.12	99.27±6.25
7s	>10	>10	>10	98.58±3.09
7t	>10	>10	>10	96.06±3.90
7u	>10	3.15±0.23	>10	101.8±2.72
PF-1	3.52±0.49	1.88±0.21	5.93±0.82	101.2±6.86
DOX	0.59±0.09	0.69±0.10	0.44±0.03	14.42±4.44

[a] Data were expressed as mean ± SD (n= 3).

[b] Cell viability was assessed after incubation of various compounds at a concentration of 100 μM.

2.5 Compound 7m reduces intracellular malonyl-CoA and triglyceride (TG) levels

Given the best antitumor activity of spiroketopyrazoles toward HepG2 cells, this cell line was selected as a model for further biological research. Initially, the antiproliferative activities of the representative compounds **7d**, **7g**, **7j**, and **7m** were evaluated at different concentrations and time points. All the compounds were found to inhibit HepG2 cell proliferation in a concentration- and time-dependent manner, as illustrated in Fig. S2. Later, the effect of **7m** on the malonyl-CoA and TG levels in HepG2 cells was investigated because the inhibition of ACC leads to a decrease in the FASyn process. The result showed that the treatment of the cells with different

concentrations of **7m** decreased the intracellular malonyl-CoA and TG levels dose-dependently, with an approximate reduction of 31.38% and 36.71% compared to the control group at a concentration of 10 μM, respectively (Fig. 4).

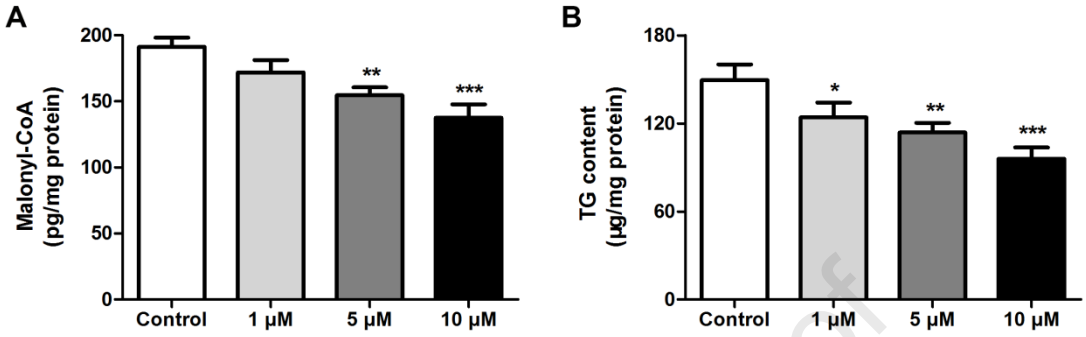

Fig. 4 Intracellular malonyl-CoA **(A)** and TG **(B)** levels after **7m** treatment. HepG2 cells were incubated with indicated concentrations of **7m** for 48 h, with the intracellular malonyl-CoA and TG extracted and quantified. Data were expressed as mean ± SD (n= 3). $^{**}P < 0.01$ and $^{***}P < 0.001$ *vs.* control group.

2.6 Palmitate rescues the cell death induced by 7m

To demonstrate that the cell proliferation inhibition was indeed caused by the lack of fatty acids, a palmitate rescue assay was performed. Palmitate is one of the most abundant dietary saturated fatty acids. Theoretically, the supplementation of the culture medium with exogenous palmitate could improve the viability of the cancer cells [25, 26]. Herein, the concentrations of palmitate were determined to be 10 μM and 25 μM due to the inhibition of cell growth at higher concentrations (Fig. 5A). On incubating the HepG2 cells with compound **7m** in a medium supplemented with palmitate for five days, the viability was significantly increased from 33.08% to 68.92% (10 μM palmitate) and 87.12% (25 μM palmitate), respectively. These data indicated that the palmitate completely eradicated the cell death induced by **7m**, strongly supporting the relationship between the antitumor activity of **7m** and its inhibitory effect on FASyn (Fig. 5B and 5C).

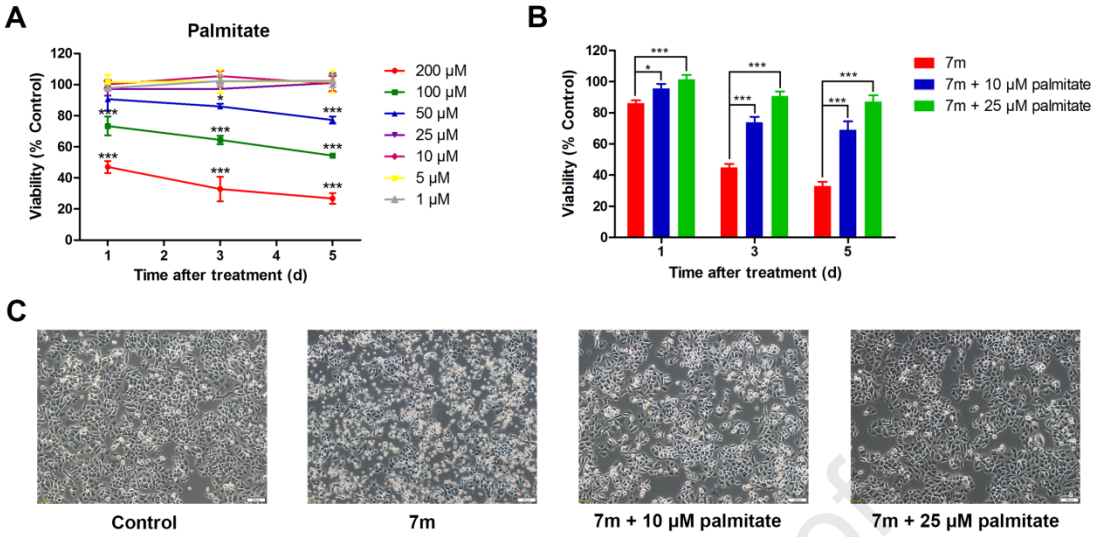

Fig. 5 Palmitate rescued the cell death induced by **7m**. (A) Cytotoxicity of palmitate on HepG2 cells. HepG2 cells were incubated with palmitate at indicated concentrations for 1, 3 and 5 days, respectively. (B) Palmitate rescued the cell death induced by **7m**. HepG2 cells were incubated with **7m** (0.5 μM) and various concentration of palmitate (0, 10, and 25 μM) for 1, 3 and 5 days, respectively. (C) Representative microphotographs of HepG2 cells after indicated treatments for 5 days (Scale bars = 100 μm). In A and B, the cell viability (% control) was determined by MTT assay. Data were expressed as mean ± SD (n= 3). **P* < 0.05, ***P* < 0.01, and ****P* < 0.001 *vs.* control group.

2.7 Compound 7m induces G0/G1 arrest in HepG2 cells

To further investigate the underlying mechanism of cytotoxicity, a DNA-based cell cycle analysis was performed using the flow cytometry technique. On treating the HepG2 cells with diverse concentrations of **7m** (1, 5, 10 μM) for 48 h, representative changes were detected in the cell cycle distribution. As shown in Fig. 6, compound **7m** resulted in a significant increase in the accumulation of cells at the G0/G1 phase from 56.24% to 88.61%, accompanied by a decrease in the cells at the S and G2/M phases from 30.18% and 13.58% to 6.48% and 4.90%, respectively. These data implied that **7m** arrested the HepG2 cells at the G0/G1 phase in a dose-dependent manner, which partly accounted for its potent anticancer activity.

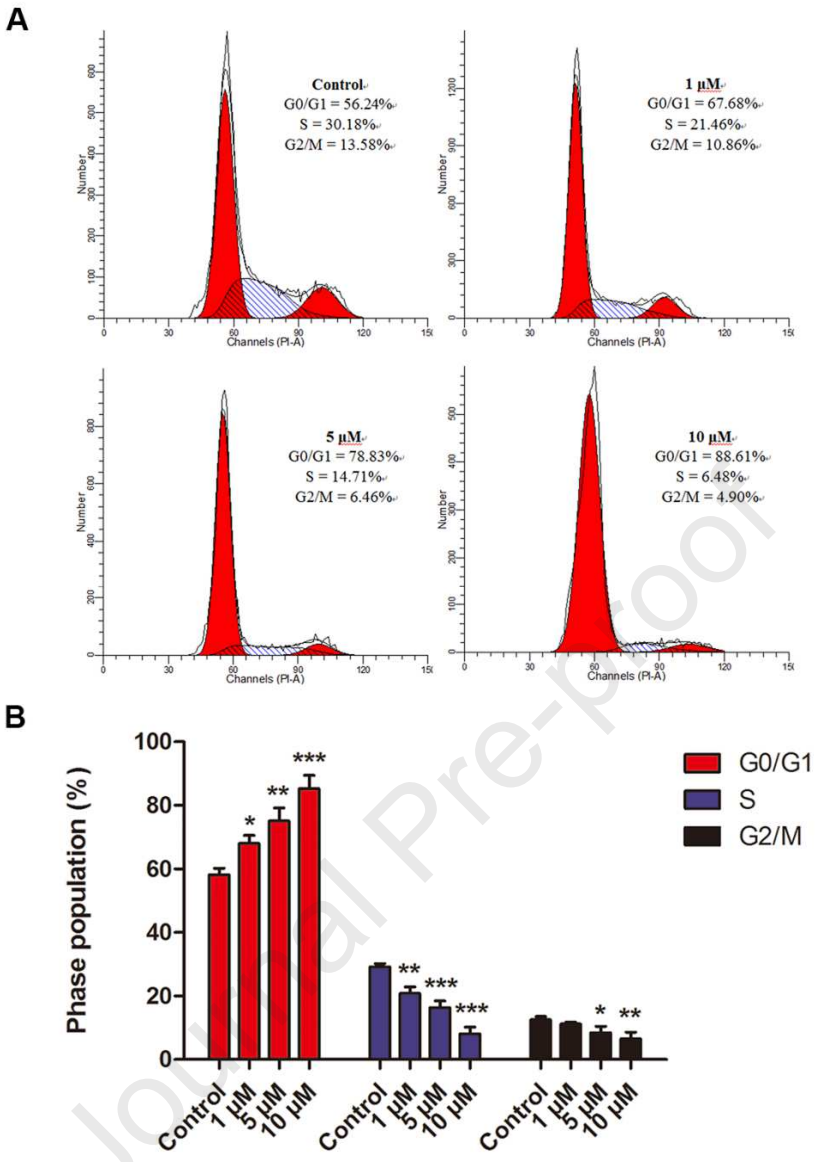

Fig. 6 Compound **7m** induced cell cycle arrest in HepG2 cells. (A) **7m** increased the distribution of cells in G0/G1 phase. After treatment with specified concentrations of **7m** for 48 h, HepG2 cells were harvested and stained with propidium iodide for flow cytometric analysis. (B) Histograms displayed the percentage of cell cycle distribution. Data were expressed as mean ± SD (n= 3). **P* < 0.05, ***P* < 0.01, and ****P* < 0.001 *vs.* control group.

2.8 Effect of compound 7m on cell cycle regulatory proteins

Based on the results of cell cycle distribution, the expressions of proteins, such as Cyclin D1 and its associated protein CDK4, that were significant for the transition from the G1 phase to the S phase were investigated using Western blot [42]. As can be seen in Fig.7, the expressions of Cyclin D1 and its associated CDK4 were decreased in a concentration-dependent manner, with approximately 43.92% and 60.76%

suppression at a concentration of 10 μM, respectively. These results suggested that the **7m**-induced G0/G1 arrest might be attributed to the down-regulation of Cyclin D1 and CDK4 proteins.

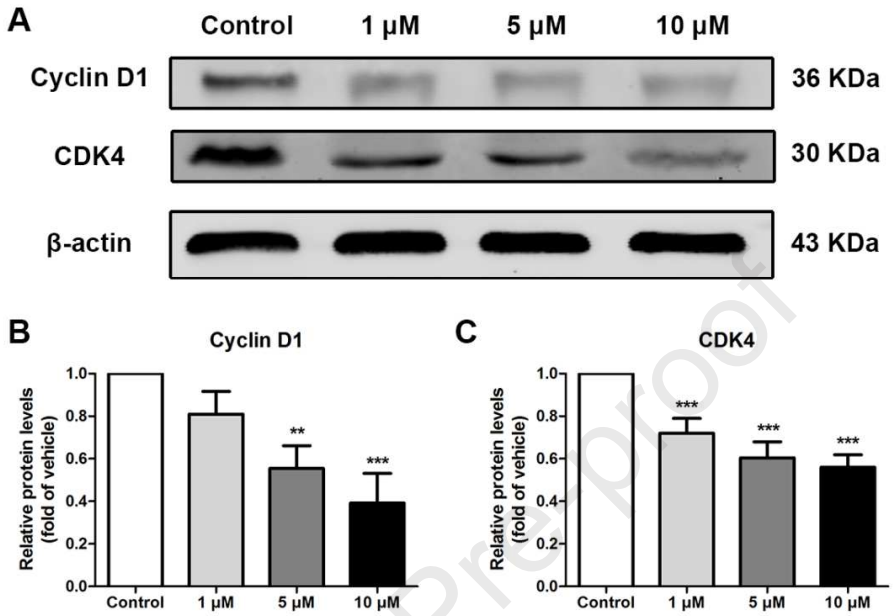

Fig. 7 Effect of compound **7m** on cell cycle regulatory proteins. (A) Western blotting analysis on the effect of **7m** on Cyclin D1 and CDK4. After treatment with indicated concentrations of **7m** for 48 h, HepG2 cells were collected and lysed to detect Cyclin D1 and CDK4, with β-actin as an internal control. (B, C) Histograms displayed the relative expression of Cyclin D1 and CDK4. Data were expressed as mean ± SD (n= 3). $^{**}P < 0.01$ and $^{***}P < 0.001$ *vs.* control group.

2.9 Compound 7m induces apoptosis in HepG2 cells

Based on the correlation between the antitumor activities of ACC inhibitors and apoptosis [25, 27], the Hoechst 33258 staining was performed to primarily investigate the nuclear morphological changes. As illustrated in Fig. 8A, the HepG2 cells treated with **7m** displayed characteristic apoptosis features, including chromatin shrinkage, nuclear fragmentation, and an increase in the brightness. Furthermore, the vehicle- or **7m**-treated HepG2 cells were further stained with Annexin V and PI to further quantitatively measure the effect of **7m** on cell apoptosis (Fig. 8B). It was found that the incubation of the HepG2 cells with **7m** induced a concentration-dependent increase in both early (from 0.19% to 41.6%) and late stages of apoptosis (from 4.03% to 45.5%) of these cells. An increase in the percentage of apoptotic cells revealed the

ability of compound **7m** in the induction of apoptosis.

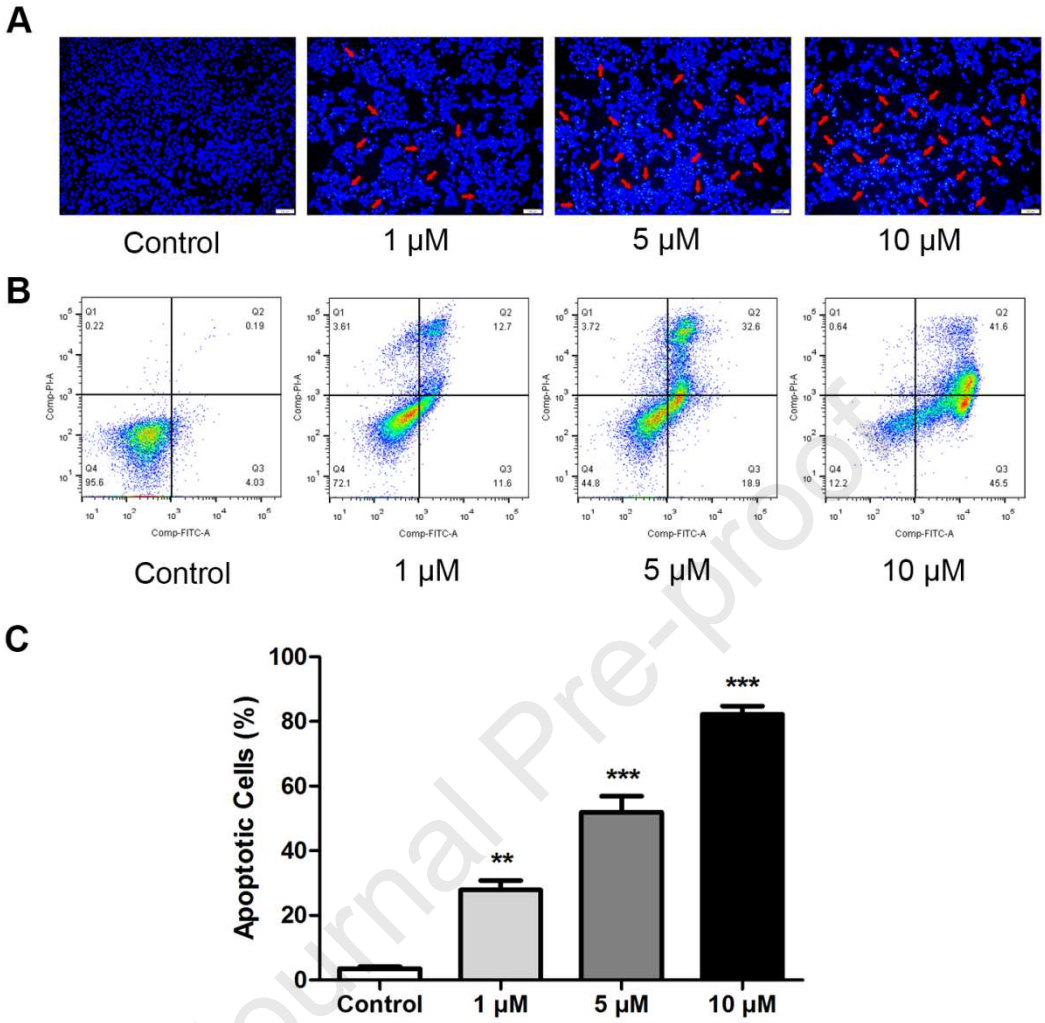

Fig. 8 Compound **7m** induced cell apoptosis. (A) Apoptotic assay by Hoechst 33258. After treatment with varying concentrations of **7m** for 48 h, HepG2 cells were stained with Hoechst 33258 and then visualized (Scale bars = 100 μM). Cells with obvious apoptosis features were marked with red arrows. (B) Apoptosis analysis using flow cytometry. HepG2 cells were exposed to **7m** for 48 h prior to staining with Annexin V-FITC/PI for flow cytometric analysis. (C) Histograms displayed the percentage of apoptotic cells. Data were expressed as mean ± SD (n= 3). $^{**}P < 0.01$ and $^{***}P < 0.001$ *vs.* control group.

2.10 Effect of compound 7m on apoptosis related proteins

To elucidate the mechanism of apoptosis induced by compound **7m**, the expressions of several apoptosis-related proteins were investigated. It has been documented that PARP, an enzyme involved in DNA repair and gene integrity monitoring, was involved in the apoptosis process induced by the inhibition of ACC

[27]. Therefore, the HepG2 cells were treated with different concentrations of **7m** (1, 5, 10 μM) to determine the protein expression of PARP in these cells. As a result, there was a remarkable increase in PARP cleavage on treatment with compound **7m** (Fig. 9E).

Since PARP is an important substrate of caspase-3, the expression of caspase-3 and Bcl-2 family proteins (Bcl-2 and Bax) were further determined [43, 44]. It was observed that the incubation of the cells with **7m** decreased the expression of anti-apoptotic Bcl-2 protein in a dose-dependent manner (Fig. 9B), while the pro-apoptotic Bax protein expression increased accordingly (Fig. 9C). Besides, the expression levels of the two cleaved forms of caspase-3 were elevated, indicating the involvement of caspase-3 activation in cell apoptosis (Fig. 9D). Therefore, compound **7m** may induce apoptosis in HepG2 cells via the mitochondrial apoptotic pathway.

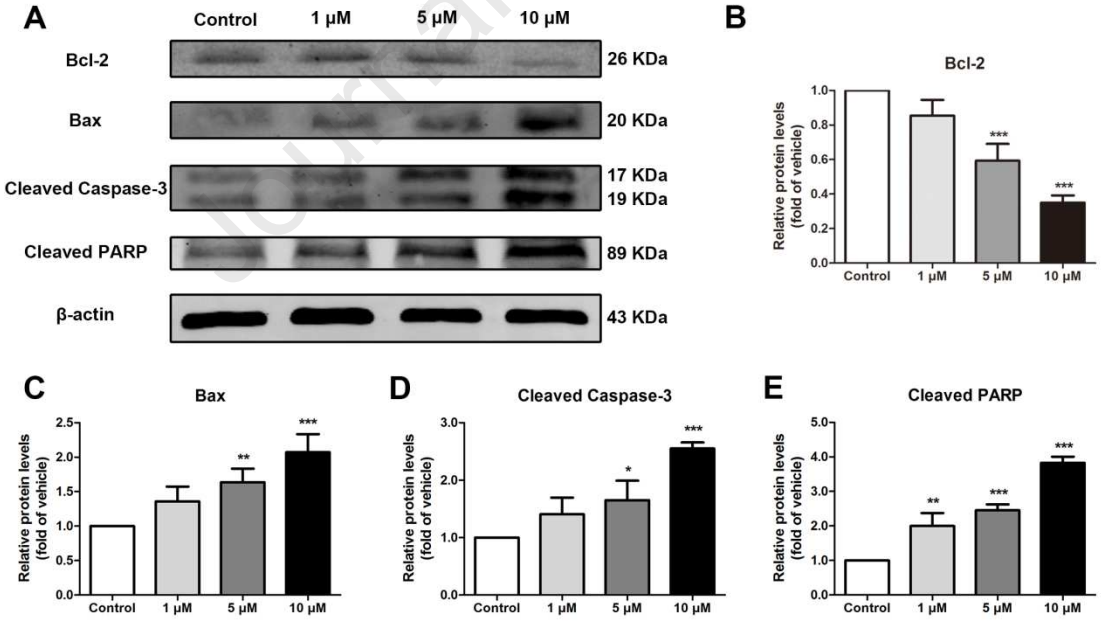

Fig. 9 Effect of compound **7m** on apoptosis related proteins. (A) Western blotting analysis on the effect of **7m** on Bcl-2, Bax, caspase-3, and PARP proteins. After treatment with **7m** for 48 h, HepG2 cells were collected and lysed to detect above-mentioned proteins, with β-actin as an internal control. (B-E) Histograms displayed the relative protein expression of Bcl-2, Bax, cleaved caspase-3, and cleaved PARP. Data were expressed as mean ± SD (n= 3). **P* < 0.05, ***P* < 0.01, and ****P* < 0.001 *vs.* control group.

2.11 Combinations of 7m and DOX lead to synergistic inhibition effects

In the course of cancer treatment, a combination of drugs is widely used to achieve synergistic therapeutic effect, dose and toxicity reduction, or drug resistance alleviation [45]. Therefore, the potential of **7m** in the combination therapy was determined by analyzing the effects of the combination of **7m** and DOX on HepG2 cell viability using the CompuSyn software[46]. As illustrated in Fig. 10, the combination of **7m** with DOX inhibited the viability of HepG2 cells in a dose-dependent manner and exhibited synergistic effects (CI < 1) at different concentrations, which highlighted the potential of compound **7m** in combination or adjuvant therapies.

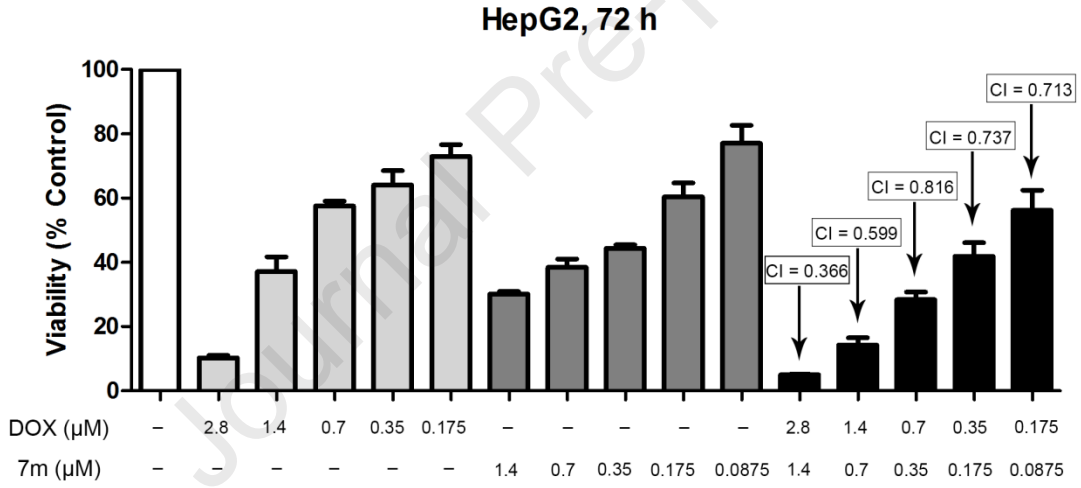

Fig. 10 Effect of **7m** and DOX combinations on HepG2 cells. Cell viability was examined after 72 h incubation of HepG2 cells with **7m** and DOX, as single agents or in combination, at the specified concentrations. CI values were calculated by CompuSyn software.

3. Conclusion

In this work, a series of new spiroketopyrazoles containing quinoline moieties were synthesized and evaluated for their anticancer activities as ACC inhibitors. At the enzyme level, compound **7j** exhibited the strongest ACC1 inhibitory activity, which is attributed to the two hydrogen bonds present between its carbonyl oxygen atom and Arg-1954'. The cellular assays showed that most of the target compounds were cytotoxic to the three cancer cells while they were essentially non-toxic to HUVEC. Among them, compound **7m** showed the highest anti-proliferative activity. The preliminary pharmacological investigation revealed that the presence of **7m** significantly reduced the levels of malonyl-CoA and TG in the HepG2 cells, and supplementation with exogenous palmitate could completely rescue the cytotoxicity, which highlighted the causal relationship between FASyn and tumor cell proliferation. Moreover, compound **7m** induced cell cycle arrest and apoptosis by regulating the cycle checkpoint proteins and mitochondrial apoptosis-related proteins, respectively. Interestingly, the combination of **7m** and DOX led to synergistic effects on the inhibition of HepG2 cell growth, suggesting its potential in combination or adjuvant therapies. Overall, these results demonstrated that the compound **7m**, acting as an ACC inhibitor, is a promising candidate for the treatment of hepatocellular carcinoma.

Journal Pre-proof

Journal Pre-proof

4. Experimental section

4.1 Chemistry

All reagents and solvents were purchased from commercial sources. The target compounds were purified by column chromatography separations on silica gel (200–300 mesh size). The melting points were measured on YRT-3 melting point apparatus and uncorrected. ^{1}H NMR and ^{13}C NMR spectra were obtained with a JNM-ECZR 400 MHz spectrometer. High-resolution mass spectra (HRMS) were recorded on a (UHR-TOF) maXis 4G instrument.

*4.1.1 General procedure for the preparation of **7a~7u***

(A) Pyruvic aldehyde (**2**, 25 mmol) was added dropwise to a solution of **1** (30 mmol) in H_2O (100 mL), and after stirring at room temperature for 2 h, the mixture was extracted with CH_2Cl_2, dried with anhydrous Na_2SO_4, and concentrated *in vacuo* to afford hydrazine **3**. Then, a 40% aqueous solution of glyoxal (25 mL) was added to a solution of **3** (62 mmol) in H_2O (100 mL). The mixture was heated at reflux for 5 h and extracted with ethyl acetate. The organic phase was dried, filtered, and concentrated to give **4** as yellow solid. Tetrahydropyrrole (8 mmol) was added to a solution of **4** (24 mmol) in MeOH (45 mL), and after stirring at room temperature for 2 h, 1-(N-Boc)-4-piperidone (28 mmol) was subsequently added, with the mixture heated at reflux for 24 h. The mixture was concentrated *in vacuo* and purified via column chromatography to give **5**. The Boc-protecting group was removed using trifluoroacetic acid in CH_2Cl_2 to provide **6**. Finally, appropriate quinoline-4-carboxylic acid derivatives (1 mmol) was added to the mixture of **6** (1.1 mmol), HATU (1.2 mmol), and triethylamine (0.2 mL) in DMF (10 mL). The mixture was stirred at room temperature overnight, and then added to ice water. The resulting precipitate was filtered, dried, and purified by column chromatography to give target compounds **7a~7m** and **7q~7u**.

(B) A mixture of **7r** (1mmol) and amine solution (2 mL) was stirred at reflux for 2 h. After cooling to room temperature, the mixture was added to water and extracted with CH_2Cl_2. The organic layers were dried, filtered, and concentrated *in vacuo*. The crude product was purified by column chromatography to yield target compounds **7n~7p**.

*2'-(tert-butyl)-1-(2-phenylquinoline-4-carbonyl)-2'H-spiro[piperidine-4,5'-pyrano[3,2-c]pyrazol]-7'(6'H)-one (**7a**)*

The product was obtained as white solid, yield 85%, m.p. 161.5 – 162.5 °C. ^{1}H NMR (400 MHz, $CDCl_3$): δ 8.24 (d, J = 8.5 Hz, 1H), 8.16 (dd, J = 6.6, 4.6 Hz, 2H), 7.84 (dd, J = 8.2, 3.3 Hz, 1H), 7.77 (dd, J = 9.5, 4.7 Hz, 2H), 7.64 – 7.45 (m, 4H), 7.23 (d, J = 3.0 Hz, 1H), 4.74 (t, J = 8.0 Hz, 1H), 3.44 – 3.35 (m, 2H), 3.25 (t, J = 11.3 Hz, 1H), 2.76 – 2.64 (m, 2H), 2.38 – 2.26 (m, 1H), 1.98 (t, J = 15.2 Hz, 1H), 1.89 – 1.79 (m, 1H), 1.64 (s, 1H), 1.59 (s, 9H). ^{13}C NMR (100 MHz, $CDCl_3$): δ 185.5, 167.1, 157.1, 156.9, 148.3, 147.0, 143.2, 138.8, 138.8, 134.2, 130.5, 130.4, 130.3, 129.9, 129.8, 129.0, 127.5, 127.4, 124.3, 124.0, 123.2, 123.0, 115.7, 112.3, 80.6, 80.5, 60.9, 49.2, 42.8, 42.7, 37.1, 34.8, 34.5, 34.0, 33.8, 29.6. HRMS *m/z* calcd for $C_{30}H_{30}N_4O_3$ $[M + H]^+$ 495.2391, found 495.2388.

*2'-(tert-butyl)-1-(2-(p-tolyl)quinoline-4-carbonyl)-2'H-spiro[piperidine-4,5'-pyrano[3,2-c]pyrazol]-7'(6'H)-one (**7b**)*

The product was obtained as yellow solid, yield 80%, m.p. 164.5 – 165.5 °C. ^{1}H NMR (400 MHz, $CDCl_3$): δ 8.22 (d, J = 8.3 Hz, 1H), 8.06 (dd, J = 8.1, 4.4 Hz, 2H), 7.82 – 7.74 (m, 3H), 7.56 (dd, J = 16.4, 8.0 Hz, 1H), 7.34 (dd, J = 7.9, 4.0 Hz, 2H), 7.23 (d, J = 2.8 Hz, 1H), 4.75 (t, J = 8.0 Hz, 1H), 3.47 – 3.31 (m, 2H), 3.24 (t, J = 12.2 Hz, 1H), 2.76 – 2.64 (m, 2H), 2.44 (s, 3H), 2.38 – 2.27 (m, 1H), 1.97 (t, J = 14.7 Hz, 1H), 1.88 – 1.80 (m, 1H), 1.64 (s, 1H), 1.59 (s, 9H). ^{13}C NMR (100 MHz, $CDCl_3$): δ 185.6, 167.2, 157.1, 156.9, 148.4, 147.0, 142.9, 140.0, 135.9, 134.1, 130.4, 130.2,

129.7, 127.3, 127.2, 127.1, 124.2, 123.9, 123.0, 122.8, 115.5, 112.3, 80.6, 80.5, 60.9, 49.1, 42.8, 42.6, 37.1, 34.7, 34.5, 33.9, 33.8, 29.5, 21.3. HRMS *m/z* calcd for $C_{31}H_{32}N_4O_3$ $[M + H]^+$ 509.2547, found 509.2557.

*2'-(tert-butyl)-1-(2-(o-tolyl)quinoline-4-carbonyl)-2'H-spiro[piperidine-4,5'-pyrano[3,2-c]pyrazol]-7'(6'H)-one (**7c**)*

The product was obtained as yellow solid, yield 75%, m.p. 159.5 – 160.5 °C. ^{1}H NMR (400 MHz, $CDCl_3$): δ 8.24 (d, J = 8.2 Hz, 1H), 7.91 – 7.74 (m, 2H), 7.63 (dd, J = 16.0, 8.6 Hz, 1H), 7.48 (t, J = 12.5 Hz, 2H), 7.40 – 7.30 (m, 3H), 7.24 (d, J = 2.8 Hz, 1H), 4.74 (t, J = 13.5 Hz, 1H), 3.54 – 3.22 (m, 3H), 2.79 – 2.61 (m, 2H), 2.43 (s, 3H), 2.32 (t, J = 12.2 Hz, 1H), 2.01 (t, J = 16.0 Hz, 1H), 1.89 – 1.74 (m, 1H), 1.64 (s, 1H), 1.59 (s, 9H). ^{13}C NMR (100 MHz, $CDCl_3$): δ 185.5, 167.0, 159.9, 148.0, 147.0, 142.3, 139.7, 135.9, 134.1, 131.0, 130.4, 130.3, 130.2, 129.7, 128.9, 127.6, 127.4, 126.1, 124.4, 124.1, 122.8, 122.6, 118.8, 112.3, 80.6, 80.5, 60.9, 49.1, 42.8, 42.7, 37.1, 34.8, 34.4, 33.9, 29.5, 20.4. HRMS *m/z* calcd for $C_{31}H_{32}N_4O_3$ $[M + H]^+$ 509.2547, found 509.2561.

*2'-(tert-butyl)-1-(2-(4-chlorophenyl)quinoline-4-carbonyl)-2'H-spiro[piperidine-4,5'-pyrano[3,2-c]pyrazol]-7'(6'H)-one (**7d**)*

The product was obtained as white solid, yield 78%, m.p. 222.5 – 223.5 °C. ^{1}H NMR (400 MHz, $CDCl_3$): δ 8.22 (d, J = 8.3 Hz, 1H), 8.12 (dd, J = 8.5, 5.7 Hz, 2H), 7.86 – 7.71 (m, 3H), 7.60 (dd, J = 16.8, 7.7 Hz, 1H), 7.51 (dd, J = 8.6, 4.1 Hz, 2H), 7.23 (d, J = 4.8 Hz, 1H), 4.75 (t, J = 11.3 Hz, 1H), 3.49 – 3.31 (m, 2H), 3.23 (t, J = 12.2 Hz, 1H), 2.77 – 2.65 (m, 2H), 2.34 (t, J = 11.4 Hz, 1H), 1.99 (t, J = 14.5 Hz, 1H), 1.88 – 1.74 (m, 1H), 1.64 (s, 1H), 1.59 (s, 9H). ^{13}C NMR (100 MHz, $CDCl_3$): δ 185.5, 166.9, 162.1, 155.8, 155.6, 148.1, 147.0, 143.4, 136.1, 134.1, 130.7, 130.5, 130.3, 129.1, 128.7, 127.7, 127.5, 124.3, 124.0, 123.2, 123.0, 115.3, 115.2, 112.3, 80.6, 80.4,

60.9, 49.1, 42.8, 42.7, 37.1, 34.7, 34.5, 34.0, 33.8, 29.5. HRMS *m/z* calcd for $C_{30}H_{29}ClN_4O_3$ $[M + H]^+$ 529.2001, found 529.1991.

*2'-(tert-butyl)-1-(2-(2-chlorophenyl)quinoline-4-carbonyl)-2'H-spiro[piperidine-4,5'-pyrano[3,2-c]pyrazol]-7'(6'H)-one (**7e**)*

The product was obtained as yellow solid, yield 68%, m.p. 216.5 – 217.5 °C. ^{1}H NMR (400 MHz, $CDCl_3$): δ 8.27 (d, J = 8.1 Hz, 1H), 7.94 – 7.77 (m, 2H), 7.76 – 7.60 (m, 3H), 7.52 (d, J = 7.1 Hz, 1H), 7.48 – 7.38 (m, 2H), 7.24 (d, J = 3.5 Hz, 1H), 4.74 (t, J = 5.6 Hz, 1H), 3.49 – 3.34 (m, 3H), 2.80 – 2.61 (m, 2H), 2.33 (t, J = 12.1 Hz, 1H), 2.04 (t, J = 16.0 Hz, 1H), 1.92 – 1.77 (m, 1H), 1.65 (s, 1H), 1.59 (s, 9H). ^{13}C NMR (100 MHz, $CDCl_3$): δ 185.5, 166.8, 156.9, 148.2, 147.0, 141.7, 138.8, 134.1, 132.1, 131.7, 131.6, 130.3, 130.1, 128.0, 127.8, 127.4, 124.6, 124.2, 123.2, 123.1, 119.4, 112.3, 80.7, 80.5, 60.9, 49.2, 42.7, 37.2, 35.0, 34.3, 33.9, 29.5. HRMS *m/z* calcd for $C_{30}H_{29}ClN_4O_3$ $[M + H]^+$ 529.2001, found 529.1996.

*2'-(tert-butyl)-1-(2-(4-fluorophenyl)quinoline-4-carbonyl)-2'H-spiro[piperidine-4,5'-pyrano[3,2-c]pyrazol]-7'(6'H)-one (**7f**)*

The product was obtained as white solid, yield 75%, m.p. > 240 °C. ^{1}H NMR (400 MHz, $CDCl_3$): δ 8.22 (d, J = 8.0 Hz, 1H), 8.20 – 8.13 (m, 2H), 7.86 – 7.70 (m, 3H), 7.59 (dd, J = 16.3, 9.2 Hz, 1H), 7.24 (d, J = 5.0 Hz, 3H), 4.75 (t, J = 12.1 Hz, 1H), 3.49 – 3.31 (m, 2H), 3.23 (t, J = 12.1 Hz, 1H), 2.77 – 2.65 (m, 2H), 2.34 (t, J = 11.9 Hz, 1H), 1.99 (t, J = 14.5 Hz, 1H), 1.87 – 1.80 (m, 1H), 1.64 (s, 1H), 1.59 (s, 9H). ^{13}C NMR (100 MHz, $CDCl_3$): δ 185.6, 167.0, 162.8, 155.8, 148.2, 147.0, 143.3, 134.8, 134.1, 130.7, 130.5, 130.2, 129.4, 127.6, 127.4, 124.3, 124.0, 123.0, 116.1, 115.8, 115.4, 112.4, 80.6, 80.5, 60.9, 49.1, 42.9, 42.7, 37.1, 34.7, 34.5, 34.0, 33.8, 29.5. HRMS *m/z* calcd for $C_{30}H_{29}FN_4O_3$ $[M + H]^+$ 513.2296, found 513.2307.

*1-(2-(4-bromophenyl)quinoline-4-carbonyl)-2'-(tert-butyl)-2'H-spiro[piperidine-4,5'-pyrano[3,2-c]pyrazol]-7'(6'H)-one (**7g**)*

The product was obtained as yellow solid, yield 70%, m.p. 171.5 – 172.5 °C. ^{1}H NMR (400 MHz, $CDCl_3$): δ 8.22 (d, J = 8.3 Hz, 1H), 8.10 – 8.00 (m, 2H), 7.85 – 7.70 (m, 3H), 7.67 (dd, J = 7.8, 2.7 Hz, 2H), 7.60 (dd, J = 15.9, 8.2 Hz, 1H), 7.23 (d, J = 4.0 Hz, 1H), 4.74 (t, J = 11.0 Hz, 1H), 3.50 – 3.32 (m, 2H), 3.22 (t, J = 11.2 Hz, 1H), 2.82 – 2.61 (m, 2H), 2.34 (t, J = 8.0 Hz, 1H), 1.98 (t, J = 13.6 Hz, 1H), 1.91 – 1.79 (m, 1H), 1.74 (s, 1H), 1.59 (s, 9H). ^{13}C NMR (100 MHz, $CDCl_3$): δ 185.5, 167.0, 155.9, 155.7, 148.2, 147.0, 143.3, 137.6, 134.1, 132.1, 130.7, 130.5, 130.3, 129.0, 127.7, 127.6, 124.3, 124.0, 123.2, 123.0, 115.3, 112.3, 80.6, 80.5, 60.9, 49.1, 42.8, 42.7, 37.2, 34.7, 34.5, 34.0, 33.8, 29.5. HRMS *m/z* calcd for $C_{30}H_{29}BrN_4O_3$ $[M + H]^+$ 573.1496, found 573.1493.

*2'-(tert-butyl)-1-(2-(4-methoxyphenyl)quinoline-4-carbonyl)-2'H-spiro[piperidine-4,5'-pyrano[3,2-c]pyrazol]-7'(6'H)-one (**7h**)*

The product was obtained as white solid, yield 73%, m.p. 218.5 – 219.5 °C. ^{1}H NMR (400 MHz, $CDCl_3$): δ 8.19 (d, J = 8.3 Hz, 1H), 8.13 (dd, J = 8.6, 5.1 Hz, 2H), 7.85 – 7.69 (m, 3H), 7.55 (dd, J = 15.4, 8.3 Hz, 1H), 7.23 (d, J = 3.3 Hz, 1H), 7.05 (dd, J = 8.7, 3.8 Hz, 2H), 4.74 (t, J = 8.6 Hz, 1H), 3.89 (s, 3H), 3.50 – 3.31 (m, 2H), 3.25 (t, J = 11.4 Hz, 1H), 2.76 – 2.64 (m, 2H), 2.33 (t, J = 9.6 Hz, 1H), 1.97 (t, J = 15.1 Hz, 1H), 1.89 – 1.76 (m, 1H), 1.64 (s, 1H), 1.58 (s, 9H). ^{13}C NMR (100 MHz, $CDCl_3$): δ 185.6, 167.2, 161.2, 161.1, 156.6, 156.5, 148.3, 147.0, 142.9, 134.1, 131.3, 131.2, 130.4, 130.3, 130.1, 128.9, 127.1, 126.9, 124.2, 123.9, 122.8, 122.6, 115.2, 114.3, 114.3, 112.3, 80.6, 80.5, 60.9, 55.4, 49.2, 42.8, 42.6, 37.1, 34.7, 34.5, 34.0, 33.8, 29.5. HRMS *m/z* calcd for $C_{31}H_{32}N_4O_4$ $[M + H]^+$ 525.2496, found 525.2489.

*2'-(tert-butyl)-1-(2-(3,4-dimethoxyphenyl)quinoline-4-carbonyl)-2'H-spiro[piperidine-4,5'-pyrano[3,2-c]pyrazol]-7'(6'H)-one (**7i**)*

The product was obtained as yellow solid, yield 85%, m.p. 169.5 – 170.5 °C. ^{1}H NMR (400 MHz, $CDCl_3$): δ 8.23 (s, 1H), 7.87 (d, J = 9.7 Hz, 1H), 7.82 – 7.71 (m, 3H), 7.66 (d, J = 8.4 Hz, 1H), 7.59 – 7.52 (m, 1H), 7.23 (d, J = 6.3 Hz, 1H), 7.01 (dd, J = 8.4, 5.5 Hz, 1H), 4.75 (t, J = 12.2 Hz, 1H), 4.06 (s, 3H), 3.97 (s, 3H), 3.48 – 3.32 (m, 2H), 3.24 (t, J = 12.1 Hz, 1H), 2.79 – 2.62 (m, 2H), 2.34 (t, J = 12.0 Hz, 1H), 1.98 (t, J = 14.3 Hz, 1H), 1.88 – 1.79 (m, 1H), 1.64 (s, 1H), 1.59 (s, 9H). ^{13}C NMR (100 MHz, $CDCl_3$): δ 185.6, 167.2, 156.6, 156.4, 150.7, 150.7, 149.4, 149.4, 148.2, 147.0, 142.9, 134.1, 131.6, 131.5, 130.4, 130.3, 130.1, 127.2, 127.0, 124.2, 123.9, 122.9, 122.7, 120.3, 120.3, 115.4, 115.3, 112.4, 111.0, 110.2, 80.6, 80.5, 60.9, 56.0, 56.0, 49.1, 42.8, 42.7, 37.1, 34.7, 34.4, 34.0, 33.8, 29.5. HRMS *m/z* calcd for $C_{32}H_{34}N_4O_5$ $[M + H]^+$ 555.2602, found 555.2586.

*1-(2-(4-aminophenyl)quinoline-4-carbonyl)-2'-(tert-butyl)-2'H-spiro[piperidine-4,5'-pyrano[3,2-c]pyrazol]-7'(6'H)-one (**7j**)*

The product was obtained as yellow solid, yield 55%, m.p. > 240 °C. ^{1}H NMR (400 MHz, $CDCl_3$): δ 8.23 (d, J = 10.0 Hz, 1H), 8.03 (dd, J = 8.4, 6.9 Hz, 2H), 7.78 – 7.69 (m, 3H), 7.53 (dd, J = 15.9, 7.7 Hz, 1H), 7.24 (d, J = 2.7 Hz, 1H), 6.81 (dd, J = 8.6, 3.4 Hz, 2H), 4.74 (t, J = 12.0 Hz, 1H), 3.48 – 3.31 (m, 2H), 3.25 (t, J = 11.7 Hz, 1H), 2.76 – 2.63 (m, 2H), 2.33 (t, J = 16.0 Hz, 1H), 1.97 (t, J = 15.9 Hz, 1H), 1.88 – 1.77 (m, 1H), 1.64 (s, 1H), 1.59 (s, 9H). ^{13}C NMR (100 MHz, $CDCl_3$): δ 185.8, 167.5, 157.1, 156.9, 148.5, 148.4, 147.1, 142.8, 142.7, 134.2, 130.4, 130.3, 130.0, 128.9, 126.8, 126.7, 124.3, 124.0, 122.8, 122.6, 115.2, 112.5, 80.8, 80.6, 61.0, 49.3, 42.9, 42.8, 37.2, 34.9, 34.6, 34.1, 33.9, 29.7. HRMS *m/z* calcd for $C_{30}H_{31}N_5O_3$ $[M + H]^+$ 510.2500, found 510.2504.

*2'-(tert-butyl)-1-(2-(4-(dimethylamino)phenyl)quinoline-4-carbonyl)-2'H-spiro[piperidine-4,5'-pyrano[3,2-c]pyrazol]-7'(6'H)-one (**7k**)*

The product was obtained as red solid, yield 55%, m.p. 199.5 – 200.5 °C. ^{1}H NMR (400 MHz, $CDCl_3$): δ 8.19 (d, J = 9.1 Hz, 1H), 8.10 (dd, J = 8.6, 4.8 Hz, 2H), 7.78 – 7.66 (m, 3H), 7.49 (dd, J = 15.6, 8.1 Hz, 1H), 7.23 (d, J = 1.9 Hz, 1H), 6.83 (dd, J = 9.0, 3.5 Hz, 2H), 4.73 (t, J = 7.6 Hz, 1H), 3.44 – 3.35 (m, 2H), 3.26 (t, J = 11.9 Hz, 1H), 3.06 (s, 6H), 2.79 – 2.61 (m, 2H), 2.32 (t, J = 9.6 Hz, 1H), 1.96 (t, J = 15.9 Hz, 1H), 1.88 – 1.75 (m, 1H), 1.64 (s, 1H), 1.59 (s, 9H). ^{13}C NMR (100 MHz, $CDCl_3$): δ 185.6, 167.5, 157.0, 156.9, 151.6, 148.4, 147.0, 142.5, 134.2, 130.1, 129.8, 128.5, 126.5, 126.3, 124.2, 123.9, 122.6, 115.0, 112.3, 112.1, 80.7, 80.6, 60.9, 49.2, 42.8, 42.6, 40.3, 37.1, 34.8, 34.5, 34.0, 33.9, 29.6. HRMS *m/z* calcd for $C_{32}H_{35}N_5O_3$ $[M + H]^+$ 538.2813, found 538.2811.

*2'-(tert-butyl)-1-(2-(pyridin-2-yl)quinoline-4-carbonyl)-2'H-spiro[piperidine-4,5'-pyrano[3,2-c]pyrazol]-7'(6'H)-one (**7l**)*

The product was obtained as white solid, yield 62%, m.p. 229.5 – 230.5 °C. ^{1}H NMR (400 MHz, $CDCl_3$): δ 8.81 – 8.65 (m, 2H), 8.55 (d, J = 23.0 Hz, 1H), 8.23 (d, J = 8.4 Hz, 1H), 7.97 – 7.73 (m, 3H), 7.61 (dd, J = 16.3, 8.4 Hz, 1H), 7.46 – 7.37 (m, 1H), 7.25 (d, J = 8.3 Hz, 1H), 4.76 (t, J = 8.0 Hz, 1H), 3.58 – 3.21 (m, 3H), 2.82 – 2.58 (m, 2H), 2.32 (t, J = 8.7 Hz, 1H), 1.99 (t, J = 9.6 Hz, 1H), 1.90 – 1.76 (m, 1H), 1.64 (s, 1H), 1.59 (s, 9H). ^{13}C NMR (100 MHz, $CDCl_3$): δ 185.7, 167.1, 155.6, 155.4, 149.2, 149.1, 148.1, 148.0, 147.0, 142.9, 137.1, 134.1, 130.4, 130.3, 130.2, 127.9, 127.7, 124.5, 124.4, 124.3, 124.1, 121.8, 115.7, 112.4, 112.3, 80.8, 80.5, 60.9, 49.2, 42.9, 42.6, 37.1, 34.7, 34.3, 34.0, 33.8, 29.5. HRMS *m/z* calcd for $C_{29}H_{29}N_5O_3$ $[M + H]^+$ 496.2343, found 496.2362.

*2'-(tert-butyl)-1-(2-(pyridin-4-yl)quinoline-4-carbonyl)-2'H-spiro[piperidine-4,5'-pyrano[3,2-c]pyrazol]-7'(6'H)-one (**7m**)*

The product was obtained as yellow solid, yield 65%, m.p. 154.5 – 155.5 °C. ^{1}H NMR (400 MHz, $CDCl_3$): δ 8.81 (s, 2H), 8.25 (d, J = 8.8 Hz, 1H), 8.07 (dd, J = 11.5,

5.5 Hz, 2H), 7.92 – 7.78 (m, 3H), 7.66 (dd, *J* = 17.9, 8.1 Hz, 1H), 7.24 (d, *J* = 4.8 Hz, 1H), 4.76 (t, *J* = 12.0 Hz, 1H), 3.52 – 3.34 (m, 2H), 3.21 (t, *J* = 11.7 Hz, 1H), 2.79 – 2.61 (m, 2H), 2.35 (t, *J* = 11.6 Hz, 1H), 1.99 (t, *J* = 12.9 Hz, 1H), 1.90 – 1.80 (m, 1H), 1.61 (s, 1H), 1.59 (s, 9H). ^{13}C NMR (100 MHz, $CDCl_3$): *δ* 185.5, 166.7, 154.3, 154.1, 150.4, 148.4, 148.3, 146.9, 145.9, 143.6, 134.1, 130.9, 130.8, 130.7, 128.5, 128.3, 124.3, 124.1, 123.8, 123.6, 121.5, 115.3, 115.2, 112.3, 80.5, 80.4, 60.9, 49.1, 42.8, 42.7, 37.2, 34.6, 34.5, 33.9, 33.7, 29.5. HRMS *m/z* calcd for $C_{29}H_{29}N_5O_3$ $[M + H]^+$ 496.2343, found 496.2356.

*2'-(tert-butyl)-1-(2-(piperazin-1-yl)quinoline-4-carbonyl)-2'H-spiro[piperidine-4,5'-pyrano[3,2-c]pyrazol]-7'(6'H)-one (**7n**)*

The product was obtained as yellow solid, yield 62%, m.p. 166.5 – 167.5 °C. ^{1}H NMR (400 MHz, $CDCl_3$): *δ* 7.72 (d, *J* = 8.4 Hz, 1H), 7.60 – 7.49 (m, 2H), 7.23 (d, *J* = 6.9 Hz, 2H), 6.90 (d, *J* = 27.3 Hz, 1H), 4.67 (t, *J* = 13.0 Hz, 1H), 3.91 – 3.60 (m, 4H), 3.44 – 3.19 (m, 3H), 3.16 – 3.05 (m, 4H), 2.76 – 2.59 (m, 2H), 2.30 (t, *J* = 13.0 Hz, 1H), 1.95 (t, *J* = 12.0 Hz, 1H), 1.83 – 1.74 (m, 1H), 1.64 (s, 1H), 1.59 (s, 9H). ^{13}C NMR (100 MHz, $CDCl_3$): *δ* 185.7, 167.4, 156.6, 156.4, 147.9, 147.0, 144.0, 134.1, 130.5, 130.3, 127.4, 124.0, 123.7, 123.6, 123.4, 119.1, 119.0, 112.4, 112.3, 106.4, 106.2, 80.6, 80.5, 60.9, 49.4, 49.2, 45.1, 45.1, 42.7, 42.6, 37.0, 34.6, 34.4, 33.9, 29.5. HRMS *m/z* calcd for $C_{28}H_{34}N_6O_3$ $[M + H]^+$ 503.2765, found 503.2789.

*2'-(tert-butyl)-1-(2-(4-methylpiperazin-1-yl)quinoline-4-carbonyl)-2'H-spiro[piperidine-4,5'-pyrano[3,2-c]pyrazol]-7'(6'H)-one (**7o**)*

The product was obtained as yellow solid, yield 65%, m.p. 161.5 – 162.5 °C. ^{1}H NMR (400 MHz, $CDCl_3$): *δ* 7.71 (d, *J* = 8.4 Hz, 1H), 7.61 – 7.44 (m, 2H), 7.23 (d, *J* = 7.8 Hz, 2H), 6.90 (d, *J* = 25.2 Hz, 1H), 4.67 (t, *J* = 13.1 Hz, 1H), 3.91 – 3.67 (m, 4H), 3.46 – 3.12 (m, 3H), 2.78 – 2.64 (m, 2H), 2.62 – 2.51 (m, 4H), 2.38 (s, 3H), 2.29 (t, *J* = 11.9 Hz, 1H), 1.98 (t, *J* = 14.6 Hz, 1H), 1.85 – 1.75 (m, 1H), 1.64 (s, 1H), 1.59 (s,

9H). ^{13}C NMR (100 MHz, $CDCl_3$): δ 185.7, 167.5, 156.6, 156.5, 148.1, 148.0, 147.0, 143.9, 134.1, 130.4, 130.2, 127.2, 124.0, 123.7, 123.3, 123.1, 119.0, 118.8, 112.4, 112.3, 106.4, 106.2, 80.6, 80.5, 60.9, 54.8, 49.1, 46.1, 44.8, 42.7, 42.6, 37.0, 34.6, 34.4, 33.9, 29.5. HRMS *m/z* calcd for $C_{29}H_{36}N_6O_3$ $[M + H]^+$ 517.2922, found 517.2931.

*2'-(tert-butyl)-1-(2-morpholinoquinoline-4-carbonyl)-2'H-spiro[piperidine-4,5'-pyrano[3,2-c]pyrazol]-7'(6'H)-one (**7p**)*

The product was obtained as yellow solid, yield 72%, m.p. 167.5 – 168.5 °C. ^{1}H NMR (400 MHz, $CDCl_3$): δ 7.74 (d, J = 3.9 Hz, 1H), 7.64 – 7.48 (m, 2H), 7.30 (d, J = 7.5 Hz, 1H), 7.23 (d, J = 8.7 Hz, 1H), 6.89 (d, J = 25.4 Hz, 1H), 4.68 (t, J = 13.0 Hz, 1H), 3.85 (d, J = 4.8 Hz, 4H), 3.73 (d, J = 0.6 Hz, 4H), 3.44 – 3.30 (m, 2H), 3.22 (t, J = 16.1 Hz, 1H), 2.76 – 2.59 (m, 2H), 2.30 (t, J = 12.3 Hz, 1H), 1.99 (t, J = 9.6 Hz, 1H), 1.83 – 1.75 (m, 1H), 1.65 (s, 1H), 1.59 (s, 9H). ^{13}C NMR (100 MHz, $CDCl_3$): δ 185.8, 167.5, 156.9, 147.1, 144.2, 134.2, 130.6, 127.4, 124.2, 123.9, 123.6, 119.3, 119.1, 112.5, 112.4, 106.3, 106.1, 80.7, 80.7, 66.9, 61.0, 49.3, 45.5, 42.9, 42.7, 37.1, 34.8, 34.5, 34.0, 29.7. HRMS *m/z* calcd for $C_{28}H_{33}N_5O_4$ $[M + H]^+$ 504.2605, found 504.2616.

*2'-(tert-butyl)-1-(2-methylquinoline-4-carbonyl)-2'H-spiro[piperidine-4,5'-pyrano[3,2-c]pyrazol]-7'(6'H)-one (**7q**)*

The product was obtained as white solid, yield 65%, m.p. 226.5 – 227.5 °C. ^{1}H NMR (400 MHz, $CDCl_3$): δ 8.09 (d, J = 8.3 Hz, 1H), 7.80 – 7.69 (m, 2H), 7.55 (dd, J = 15.6, 7.8 Hz, 1H), 7.26 (s, 1H), 7.24 (s, 1H), 4.71 (t, J = 9.6 Hz, 1H), 3.46 – 3.28 (m, 2H), 3.18 (t, J = 13.5 Hz, 1H), 2.77 (s, 3H), 2.73 – 2.63 (m, 2H), 2.32 (t, J = 12.2 Hz, 1H), 1.98 (t, J = 17.6 Hz, 1H), 1.86 – 1.76 (m, 1H), 1.64 (s, 1H), 1.59 (s, 9H). ^{13}C NMR (100 MHz, $CDCl_3$): δ 185.6, 167.0, 158.9, 158.7, 147.8, 147.0, 142.5, 134.1, 130.3, 130.1, 129.2, 126.9, 126.7, 124.2, 123.9, 122.4, 122.2, 118.6, 118.5, 112.3,

80.6, 80.5, 60.9, 49.1, 42.7, 42.6, 37.0, 34.7, 34.4, 33.8, 29.5, 25.3. HRMS *m/z* calcd for $C_{25}H_{28}N_4O_3$ $[M + H]^+$ 433.2234, found 433.2244.

*2'-(tert-butyl)-1-(2-chloroquinoline-4-carbonyl)-2'H-spiro[piperidine-4,5'-pyrano[3,2-c]pyrazol]-7'(6'H)-one (**7r**)*

The product was obtained as white solid, yield 80%, m.p. 219.5 – 220.5 °C. 20 ^oC, ^1H NMR (400 MHz, DMSO-d_6): δ 8.02 (d, J = 8.4 Hz, 1H), 7.89 (t, J = 7.6 Hz, 2H), 7.80 – 7.72 (m, 2H), 7.65 (d, J = 23.6 Hz, 1H), 4.40 (d, J = 13.2 Hz, 1H), 3.28 (s, 3H), 2.75 (s, 2H), 2.51 (t, J = 2.0 Hz, 1H), 2.11 (d, J = 13.6 Hz, 1H), 1.81 (s, 2H), 1.51 (s, 9H). ^{13}C NMR (100 MHz, DMSO-d_6): δ 186.2, 164.6, 150.1, 147.9, 147.4, 146.7, 134.0, 132.1, 129.0, 128.8, 125.7, 125.5, 123.5,123.3, 119.4, 114.2, 81.4, 81.3, 60.9, 48.9, 48.6, 43.0,42.9, 37.5, 37.4, 34.3, 33.9, 33.3,33.2, 29.6. 85 ^oC, ^1H NMR (400 MHz, DMSO-d_6): δ 8.00 (d, J = 8.8 Hz, 1H), 7.87 (t, J = 8.0 Hz, 2H), 7.69 (q, J = 7.6 Hz, 2H), 7.58 (s, 1H), 4.36 (d, J = 12.8 Hz, 1H), 3.34 (t, J = 8.8 Hz, 2H), 3.14 (d, J = 14.0 Hz, 1H), 2.74 (d, J = 4 Hz, 2H), 2.49 (s, 1H), 2.12 (d, J = 14.4 Hz, 1H), 1.92 – 1.81 (m, 2H), 1.52 (s, 9H). ^{13}C NMR (100 MHz, DMSO-d_6): δ 185.8, 164.9, 150.1, 148.1, 147.5, 146.7, 134.4, 131.9, 129.1, 128.6, 125.6, 123.5, 119.4, 113.9, 81.4, 60.9, 49.0, 43.0, 37.6, 34.3, 33.6, 29.7. HRMS *m/z* calcd for $C_{24}H_{25}ClN_4O_3$ $[M + H]^+$ 453.1688, found 453.1699.

*2'-(tert-butyl)-1-(2-methoxyquinoline-4-carbonyl)-2'H-spiro[piperidine-4,5'-pyrano[3,2-c]pyrazol]-7'(6'H)-one (**7s**)*

The product was obtained as yellow solid, yield 65%, m.p. > 240 °C. ^1H NMR (400 MHz, $CDCl_3$): δ 7.63 (dd, J = 16.9, 7.4 Hz, 1H), 7.51 (dd, J = 20.3, 8.3 Hz, 1H), 7.42 (dd, J = 8.4, 4.0 Hz, 1H), 7.31 – 7.20 (m, 2H), 6.64 (d, J = 20.1 Hz, 1H), 4.64 (t, J = 8.7 Hz, 1H), 3.74 (s, 3H), 3.52 – 3.38 (m, 2H), 3.32 (t, J = 13.7 Hz, 1H), 2.77 – 2.60 (m, 2H), 2.30 (t, J = 12.2 Hz, 1H), 2.03 (t, J = 12.0 Hz, 1H), 1.82 – 1.73 (m, 1H), 1.66 (s, 1H), 1.59 (s, 9H). ^{13}C NMR (100 MHz, $CDCl_3$): δ 185.5, 165.6, 161.3, 147.0,

145.0, 140.3, 134.1, 131.7, 131.6, 126.3, 126.0, 122.8, 122.7, 118.3, 118.2, 117.4, 117.3, 114.9, 114.8, 112.5, 112.3, 80.6, 80.4, 77.3, 77.0, 76.7, 61.0, 53.4, 49.1, 42.7, 42.5, 37.0, 34.8, 34.5, 33.9, 33.6, 29.6. HRMS *m/z* calcd for $C_{25}H_{28}N_4O_4$ $[M + H]^+$ 449.2183, found 449.2184.

*2'-(tert-butyl)-1-(2-ethoxyquinoline-4-carbonyl)-2'H-spiro[piperidine-4,5'-pyrano[3,2-c]pyrazol]-7'(6'H)-one (**7t**)*

The product was obtained as yellow solid, yield 60%, m.p. 174.5 – 175.5 °C. ^{1}H NMR (400 MHz, $CDCl_3$): δ 7.67 – 7.58 (m, 1H), 7.52 (dd, J = 20.7, 7.9 Hz, 1H), 7.44 (dd, J = 8.5, 4.1 Hz, 1H), 7.30 – 7.21 (m, 2H), 6.63 (d, J = 18.4 Hz, 1H), 4.64 (t, J = 8.6 Hz, 1H), 4.33 (t, J = 16.9 Hz, 2H), 3.55 – 3.37 (m, 2H), 3.31 (t, J = 12.9 Hz, 1H), 2.77 – 2.57 (m, 2H), 2.30 (t, J = 8.0 Hz, 1H), 2.04 (t, J = 11.0 Hz, 1H), 1.81 – 1.73 (m, 1H), 1.66 (s, 1H), 1.59 (s, 9H), 1.37 (s, 3H). ^{13}C NMR (100 MHz, $CDCl_3$): δ 185.4, 165.6, 160.9, 147.0, 145.1, 144.9, 139.4, 134.1, 131.6, 131.5, 126.4, 126.1, 122.6, 122.4, 118.4, 118.2, 117.6, 117.5, 114.7, 114.6, 112.5, 112.3, 80.6, 80.4, 60.9, 60.9, 49.1, 49.1, 42.7, 42.5, 37.5, 37.0, 34.8, 34.5, 33.9, 33.6, 29.5, 12.6. HRMS *m/z* calcd for $C_{26}H_{30}N_4O_4$ $[M + H]^+$ 463.2340, found 463.2339.

*2'-(tert-butyl)-1-(2-isopropoxyquinoline-4-carbonyl)-2'H-spiro[piperidine-4,5'-pyrano[3,2-c]pyrazol]-7'(6'H)-one (**7u**)*

The product was obtained as white solid, yield 55%, m.p. 114.5 – 115.5 °C. ^{1}H NMR (400 MHz, $CDCl_3$): δ 7.85 (d, J = 8.3 Hz, 1H), 7.64 (dd, J = 18.3, 9.2 Hz, 2H), 7.39 (dd, J = 15.2, 7.7 Hz, 1H), 7.23 (d, J = 3.4 Hz, 1H), 6.76 (d, J = 22.6 Hz, 1H), 5.61 – 5.55 (m, 1H), 4.68 (t, J = 2.6 Hz, 1H), 3.47 – 3.20 (m, 3H), 2.78 – 2.62 (m, 2H), 2.29 (t, J = 8.6 Hz, 1H), 1.98 (t, J = 12.6 Hz, 1H), 1.85 – 1.71 (m, 1H), 1.64 (s, 1H), 1.59 (s, 9H), 1.40 (s, 6H). ^{13}C NMR (100 MHz, $CDCl_3$): δ 185.7, 166.9, 161.2, 161.1, 147.1, 145.0, 144.9, 134.3, 130.3, 130.2, 127.9, 124.8, 124.7, 124.5, 124.2, 121.2, 121.0, 112.5, 110.7, 80.8, 80.6, 68.6, 68.6, 61.0, 49.3, 49.3, 42.9, 42.7, 37.2, 34.8,

34.6, 34.1, 33.9, 29.7, 22.1. HRMS *m/z* calcd for $C_{27}H_{32}N_4O_4$ $[M + H]^+$ 477.2496, found 477.2496.

4.2 Molecular docking

This study was performed using software Sybyl-X 2.1, and the co-crystal of ACC with **PF-1** was taken from the Protein Data Bank (PDB ID: 4WYO) [30]. All water was removed and missing hydrogen atoms were added to the original structure. The ligands were energy minimized with Tripos force field and Gasteiger-Huckl charges as implement in SYBYL. The best output pose of ligand was analyzed based on hydrogen bonds and van der Waals interactions to the enzyme. The results were visualized with PyMOL.

4.3 Pharmacology

4.3.1 In vitro ACC inhibition assay

ACC inhibitory activity of compounds was assessed using a luminescent ADP detection assay according to the previous report of Harriman *et al* [35]. Briefly, 4.5 μL of assay buffer containing recombinant ACC1 (BPS Biosciences, Catalog #50200) was added to Optiplate-384 (Perkin Elmer, Catalog #6007290) followed by 0.5 μL of DMSO or DMSO containing inhibitor. After incubation at room temperature for 15 min, 5 μL of substrate mixture was added to start the reaction. The plate was incubated at room temperature for 60 min, then 10 μL ADP-Glo Reagent was added to terminate the reaction. After 40 min incubation at room temperature, 20 μL Kinase Detection Reagent was added and plates were incubated for another 40 min to convert ADP to ATP. Finally, ATP was measured using an Envision 2104 multi-label reader (Perkin Elmer, 2104-0010).

4.3.2 Cell Culture

All the cell lines were obtained from the Shanghai Cell Bank of Chinese

Academy of Sciences (Shanghai, China). A549, HepG2 and MDA-MB-231 cancer cell lines were cultured in Dulbecco's modified Eagle's medium (DMEM) supplemented with 10% fetal bovine serum (FBS), 1% streptomycin and penicillin. HUVEC were maintained in RPMI 1640 media supplemented with 10% FBS, 1% streptomycin and penicillin. The cells were cultured under standard conditions: 37 °C and 5% CO_2 in a humidified atmosphere.

4.3.3 Cell viability assay

The cytotoxicity of synthesized compounds was determined by MTT assay (Beyotime, China). Cells at density of 3×10^3 per well were seeded in 96-well plates, and after incubation for 24 h, the cells were treated with various concentrations of compounds for 72 h. At the end of treatment, an MTT solution (20 μL) was added and incubated for another 4 h. The formed formazan was dissolved with 100 μL of DMSO, with the absorbance measured at 550 nm using a microplate reader (Varioskan LUX).

4.3.4 Measurement of malonyl-CoA and TG

HepG2 cells were plated on 6-well plates and incubated with diverse concentrations of **7m** for 48 h. Then, cells were collected, washed with PBS, and lysed with 1% Triton X-100. The lysates were centrifuged at 12000 rpm at 4 °C for 15 min. The contents of malonyl-CoA and TG were measured using Elisa assay kits (Ruixin Biotech, China) and GPO-POP assay kits (Jiancheng Bio, China), respectively. To normalize the malonyl-CoA and TG levels, the protein concentration was measured by BCA protein assay kits (Beyotime, China).

4.3.5 Palmitate rescue assay

The rescue experiments were performed by adding the palmitate–BSA complex to **7m**-treated cells. For palmitate–BSA preparation, a 100 mM palmitate stock solution was prepared by dissolving 27.9 mg of sodium palmitate (Sigma-Aldrich) in

1 mL of sterile water by alternating vortexing and heating at 70 °C. Then, 200 μL from the previous palmitate solution was added to 3.8 mL of serum-free DMEM with 5% fatty acid-free BSA (Yeasen Biotech Co., Ltd.) to make a 5 mM palmitate solution. Later, 5 mM palmitate solution was shaken at 140 rpm at 40 °C for 1 h [47]. Finally, the mixture was further diluted in serum-free DMEM to obtain the required final concentrations and added to the culture medium immediately. Cell viability was performed using MTT assay, cell morphology was observed through a fluorescence microscope (Olympus IX73).

4.3.6 Cell cycle assay

HepG2 cells were plated on 6-well plates and exposed to diverse concentrations of **7m** for 48 h after they adherence. Then, cells were collected and fixed in 70% precooled ethanol overnight. Finally, cells were staining with propidium iodide/ RNase A for 30 min and subjected to flow cytometer (Facs Canto II, USA) for measurement.

4.3.7 Cell apoptosis assay

(A) Hoechst 33258 staining. HepG2 cells were seeded in 6-well plates and exposed to various concentrations of **7m** for 48 h. After treatment, cells were stained with Hoechst 33258 in dark for 20 min. The morphological images were observed under a fluorescence microscope (Olympus IX73).

(B) Annexin V-FITC/ PI apoptosis assay. HepG2 cells were plated on 6-well plates and incubated with specific concentration of **7m** for 48 h. Then, cells were harvested and stained with annexin-V-FITC and PI (KeyGen, China) protected from light. The percentages of apoptotic cells were measured by flow cytometer (Facs Canto II, USA).

4.3.8 Western blotting

HepG2 cells were exposed to the indicated concentrations of **7m** for 48 h. Then, cells were collected and lysed. The cell lysates were centrifuged at 12000 rpm for 15 min, and the supernatants were collected. The protein concentration was quantified using the BCA protein assay reagents (Beyotime, China). Protein samples were separated by SDS-PAGE and transferred onto PVDF membranes. After blocking with 5% BSA for 1 h, membranes were incubated with appropriate primary antibodies at 4 °C overnight. Finally, the membranes were incubated with a DyLight 800 labeled secondary antibody for 60 min and scanned using the Odyssey infrared imaging System (LI-COR, Inc., USA). The densitometric quantification analysis was performed by Image J.

4.3.9 Calculation of Combination Index (CI)

HepG2 cells were treated with specified concentrations of **7m** and DOX, as single agents or in combination for 72 h. The CI values were calculated the using the CompuSyn software (Version 1.0; ComboSyn Inc., USA). Based on this analysis, CI > 1, = 1, and < 1 indicate synergism, additive effect, and antagonism, respectively [43].

Acknowledgments

This study was funded by the grants from National Natural Science Foundation of China (81671744), Natural Science Foundation of Jiangsu Province (BK20171184), China Postdoctoral Science Foundation (2017M611916), and Science and Technology Planning Project of Xuzhou, China (KC20104).

Journal Pre-proof

References

[1] M.G. Vander Heiden, L.C. Cantley, C.B. Thompson, Understanding the warburg effect: The metabolic requirements of cell proliferation, Science. 324 (2009) 1029-1033.

[2] D. Hanahan, R.A. Weinberg, Hallmarks of cancer: The next generation, Cell. 144 (2011) 646-674.

[3] J.A. Menendez, R. Lupu, Fatty acid synthase and the lipogenic phenotype in cancer pathogenesis, Nat. Rev. Cancer. 7 (2007) 763-777.

[4] C.R. Santos, A. Schulze, Lipid metabolism in cancer, Febs J. 279 (2012) 2610-2623.

[5] E. Currie, A. Schulze, R. Zechner, T.C. Walther, R.V. Farese, Cellular fatty acid metabolism and cancer, Cell Metab. 18 (2013) 153-161.

[6] F. Rohrig, A. Schulze, The multifaceted roles of fatty acid synthesis in cancer, Nat. Rev. Cancer. 16 (2016) 732-749.

[7] Y. J. Tan, A. Ali, S. Y. Tee, J. T. Teo, X. Yu, M. L. Go, Y. Lam, Galloyl esters of trans-stilbenes are inhibitors of FASN with anticancer activity on non-small cell lung cancer cells, Eur. J. Med. Chem. 182 (2019) 111597.

[8] P. K. Singha, K. Mäklin, T. Vihavainen, T. Laitinen, T. J. Nevalainen, M. R. Patil, A. K. Tonduru, A. Poso, J. T. Laitinen, J. R. Savinainen，Evaluation of FASN inhibitors by a versatile toolkit reveals differences in pharmacology between human and rodent FASN preparations and in antiproliferative efficacy *in vitro vs. in situ* in human cancer cells, Eur. J. Pharm. Sci. 149 (2020) 105321.

[9] R.U. Svensson, R.J. Shaw, Lipid synthesis is a metabolic liability of non-small cell lung cancer, Cold Spring Harb. Symp. Quant. Biol. 81 (2016) 93-103.

[10] E.Q. Li, W. Zhao, C. Zhang, L.Z. Qin, S.J. Liu, Z.Q. Feng, X. Wen, C.P. Chen, Synthesis and anti-cancer activity of nd-646 and its derivatives as acetyl-coa

carboxylase 1 inhibitors, Eur. J. Pharm. Sci. 137 (2019) 105010.

[11] G. Zadra, C.F. Ribeiro, P. Chetta, Y. Ho, S. Cacciatore, X. Gao, S. Syamala, C. Bango, C. Photopoulos, Y. Huang, S. Tyekucheva, D.C. Bastos, J. Tchaicha, B. Lawney, T. Uo, L. D'Anello, A. Csibi, R. Kalekar, B. Larimer, L. Ellis, L.M. Butler, C. Morrissey, K. McGovern, V.J. Palombella, J.L. Kutok, U. Mahmood, S. Bosari, J. Adams, S. Peluso, S.M. Dehm, S.R. Plymate, M. Loda, Inhibition of de novo lipogenesis targets androgen receptor signaling in castration-resistant prostate cancer, Proc. Natl. Acad. Sci. U. S. A. 116 (2019) 631-640.

[12] L. Tong, Acetyl-coenzyme a carboxylase: Crucial metabolic enzyme and attractive target for drug discovery, Cell. Mol. Life Sci. 62 (2005) 1784-1803.

[13] X. Wu, T. Huang, Recent development in acetyl-coa carboxylase inhibitors and their potential as novel drugs, Future Med. Chem. 12 (2020) 533-561.

[14] M.P. Bourbeau, M.D. Bartberger, Recent advances in the development of acetyl-coa carboxylase (acc) inhibitors for the treatment of metabolic disease, J. Med. Chem. 58 (2015) 525-536.

[15] L.Y. Chen, Y.Q. Duan, H.Q. Wei, H.X. Ning, C.F. Bi, Y. Zhao, Y. Qin, Y.L. Li, Acetyl-coa carboxylase (acc) as a therapeutic target for metabolic syndrome and recent developments in acc1/2 inhibitors, Expert. Opin. Inv. Drug. 28 (2019) 917-930.

[16] M.A. Silvers, G.T. Robertson, C.M. Taylor, G.L. Waldrop, Design, synthesis, and antibacterial properties of dual-ligand inhibitors of acetyl-coa carboxylase, J. Med. Chem. 57 (2014) 8947-8959.

[17] C. Wang, J. Ma, N. Zhang, Q.L. Yang, Y. Jin, Y. Wang, The acetyl-coa carboxylase enzyme: A target for cancer therapy?, Expert Rev. Anticanc. 15 (2015) 667-676.

[18] S. Braig, Chemical genetics in tumor lipogenesis, Biotechnol. Adv. 36 (2018)

1724-1729.

[19] J. Saab, M.L. Santos-Zabala, M. Loda, E.C. Stack, T.J. Hollmann, Fatty acid synthase and acetyl-coa carboxylase are expressed in nodal metastatic melanoma but not in benign intracapsular nodal nevi, Am. J. Dermatopath. 40 (2018) 259-264.

[20] N. Yahagi, H. Shimano, K. Hasegawa, K. Ohashi, T. Matsuzaka, Y. Najima, M. Sekiya, S. Tomita, H. Okazaki, Y. Tamura, Y. Iizuka, K. Ohashi, R. Nagai, S. Ishibashi, T. Kadowaki, M. Makuuchi, S. Ohnishi, J. Osuga, N. Yamada, Co-ordinate activation of lipogenic enzymes in hepatocellular carcinoma, Eur. J. Cancer. 41 (2005) 1316-1322.

[21] J.V. Swinnen, F. Vanderhoydonc, A.A. Elgamal, M. Eelen, I. Vercaeren, S. Joniau, H. Van Poppel, L. Baert, K. Goossens, W. Heyns, G. Verhoeven, Selective activation of the fatty acid synthesis pathway in human prostate cancer, Int. J. Cancer. 88 (2000) 176-179.

[22] V. Chajes, M. Cambot, K. Moreau, G.M. Lenoir, V. Joulin, Acetyl-coa carboxylase alpha is essential to breast cancer cell survival, Cancer Res. 66 (2006) 5287-5294.

[23] K. Brusselmans, E. De Schrijver, G. Verhoeven, J.V. Swinnen, Rna interference-mediated silencing of the acetyl-coa-carboxylase-alpha gene induces growth inhibition and apoptosis of prostate cancer cells, Cancer Res. 65 (2005) 6719-6725.

[24] E. Petrova, A. Scholz, J. Paul, A. Sturz, K. Haike, F. Siegel, D. Mumberg, N.S. Liu, Acetyl-coa carboxylase inhibitors attenuate wnt and hedgehog signaling and suppress pancreatic tumor growth, Oncotarget. 8 (2017) 48660-48670.

[25] C. Wang, C. Xu, M. Sun, D. Luo, D.F. Liao, D. Cao, Acetyl-coa carboxylase-alpha inhibitor tofa induces human cancer cell apoptosis, Biochem.

Biophys. Res. Commun. 385 (2009) 302-306.

[26] A. Beckers, S. Organe, L. Tinunermans, K. Scheys, A. Peeters, K. Brusselmans, G. Verhoeven, J.V. Swinnen, Chemical inhibition of acetyl-coa carboxylase induces growth arrest and cytotoxicity selectively in cancer cells, Cancer Res. 67 (2007) 8180-8187.

[27] R.U. Svensson, S.J. Parker, L.J. Eichner, M.J. Kolar, M. Wallace, S.N. Brun, P.S. Lombardo, J.L. Van Nostrand, A. Hutchins, L. Vera, L. Gerken, J. Greenwood, S. Bhat, G. Harriman, W.F. Westlin, H.J. Harwood, Jr., A. Saghatelian, R. Kapeller, C.M. Metallo, R.J. Shaw, Inhibition of acetyl-coa carboxylase suppresses fatty acid synthesis and tumor growth of non-small-cell lung cancer in preclinical models, Nat. Med. 22 (2016) 1108-1119.

[28] J.S.V. Lally, S. Ghoshal, D.K. DePeralta, O. Moaven, L. Wei, R. Masia, D.J. Erstad, N. Fujiwara, V. Leong, V.P. Houde, A.E. Anagnostopoulos, A. Wang, L.A. Broadfield, R.J. Ford, R.A. Foster, J. Bates, H.L. Sun, T. Wang, H. Liu, A.S. Ray, A.K. Saha, J. Greenwood, S. Bhat, G. Harriman, W.Y. Miao, J.L. Rocnik, W.F. Westlin, P. Muti, T. Tsakiridis, H.J. Harwood, R. Kapeller, Y. Hoshida, K.K. Tanabe, G.R. Steinberg, B.C. Fuchs, Inhibition of acetyl-coa carboxylase by phosphorylation or the inhibitor nd-654 suppresses lipogenesis and hepatocellular carcinoma, Cell Metab. 29 (2019) 174-182.

[29] Q. Wei, L. Mei, Y. Yang, H. Ma, H. Chen, H. Zhang, J. Zhou, Design, synthesis and biological evaluation of novel spiro-pentacylamides as acetyl-coa carboxylase inhibitors, Bioorg. Med. Chem. 26 (2018) 3866-3874.

[30] Q. Wei, L. Mei, P. Chen, X. Yuan, H. Zhang, J. Zhou, Design, synthesis and biological evaluation of novel chroman derivatives as non-selective acetyl-coa carboxylase inhibitors, Bioorg. Chem. 101 (2020) 103943.

[31] K.D. Freeman-Cook, P. Amor, S. Bader, L.M. Buzon, S.B. Coffey, J.W. Corbett,

K.J. Dirico, S.D. Doran, R.L. Elliott, W. Esler, A. Guzman-Perez, K.E. Henegar, J.A. Houser, C.S. Jones, C. Limberakis, K. Loomis, K. McPherson, S. Murdande, K.L. Nelson, D. Phillion, B.S. Pierce, W. Song, E. Sugarman, S. Tapley, M. Tu, Z. Zhao, Maximizing lipophilic efficiency: The use of free-wilson analysis in the design of inhibitors of acetyl-coa carboxylase, J. Med. Chem. 55 (2012) 935-942.

[32] D.A. Griffith, D.W. Kung, W.P. Esler, P.A. Amor, S.W. Bagley, C. Beysen, S. Carvajal-Gonzalez, S.D. Doran, C. Limberakis, A.M. Mathiowetz, K. McPherson, D.A. Price, E. Ravussin, G.E. Sonnenberg, J.A. Southers, L.J. Sweet, S.M. Turner, F.F. Vajdos, Decreasing the rate of metabolic ketone reduction in the discovery of a clinical acetyl-coa carboxylase inhibitor for the treatment of diabetes, J. Med. Chem. 57 (2014) 10512-10526.

[33] C. Bengtsson, S. Blaho, D.B. Saitton, K. Brickmann, J. Broddefalk, O. Davidsson, T. Drmota, R. Folmer, K. Hallberg, S. Hallen, R. Hovland, E. Isin, P. Johannesson, B. Kull, L.O. Larsson, L. Lofgren, K.E. Nilsson, T. Noeske, N. Oakes, A.T. Plowright, V. Schnecke, P. Stahlberg, P. Sorme, H. Wan, E. Wellner, L. Oster, Design of small molecule inhibitors of acetyl-coa carboxylase 1 and 2 showing reduction of hepatic malonyl-coa levels in vivo in obese zucker rats, Bioorg. Med. Chem. 19 (2011) 3039-3053.

[34] V. Sharma, D.K. Mehta, R. Das, Synthetic methods of quinoline derivatives as potent anticancer agents, Mini. Rev. Med. Chem. 17 (2017) 1557-1572.

[35] G. Harriman, J. Greenwood, S. Bhat, X. Huang, R. Wang, D. Paul, L. Tong, A.K. Saha, W.F. Westlin, R. Kapeller, H.J. Harwood, Jr., Acetyl-coa carboxylase inhibition by nd-630 reduces hepatic steatosis, improves insulin sensitivity, and modulates dyslipidemia in rats, Proc. Natl. Acad. Sci. U. S. A. 113 (2016) E1796-1805.

[36] N. Alkhouri, E. Lawitz, M. Noureddin, R. DeFronzo, G.I. Shulman, Gs-0976

(firsocostat): An investigational liver-directed acetyl-coa carboxylase (acc) inhibitor for the treatment of non-alcoholic steatohepatitis (nash), Expert. Opin. Inv. Drug. 29 (2020) 135-141.

[37] J. Qiu, W. Chen, Y. Zhang, Q. Zhou, J. Chen, L. Yang, J. Gao, X. Gu, D. Tang, Assessment of quinazolinone derivatives as novel non-nucleoside hepatitis b virus inhibitors, Eur. J. Med. Chem. 176 (2019) 41-49.

[38] T.H. Huang, X. Wu, T.Y. Liu, L. An, X.X. Yin, Synthesis and anticancer activity evaluation of novel oxacalix[2]arene[2]pyrimidine derivatives, Med. Chem. Res. 28 (2019) 580-590.

[39] D.A. Griffith, R.L. Dow, K. Huard, D.J. Edmonds, S.W. Bagley, J. Polivkova, D. Zeng, C.N. Garcia-Irizarry, J.A. Southers, W. Esler, P. Amor, K. Loomis, K. McPherson, K.B. Bahnck, C. Preville, T. Banks, D.E. Moore, A.M. Mathiowetz, E. Menhaji-Klotz, A.C. Smith, S.D. Doran, D.A. Beebe, M.F. Dunn, Spirolactam-based acetyl-coa carboxylase inhibitors: Toward improved metabolic stability of a chromanone lead structure, J. Med. Chem. 56 (2013) 7110-7119.

[40] T.W. Johnson, R.A. Gallego, M.P. Edwards, Lipophilic efficiency as an important metric in drug design, J. Med. Chem. 61 (2018) 6401-6420.

[41] D.K. Glatzel, A. Koeberle, H. Pein, K. Loser, A. Stark, N. Keksel, O. Werz, R. Muller, I. Bischoff, R. Furst, Acetyl-coa carboxylase 1 regulates endothelial cell migration by shifting the phospholipid composition, J. Lipid. Res. 59 (2018) 298-311.

[42] Y. Zhang, S. Chen, C. Wei, G.O. Rankin, X. Ye, Y.C. Chen, Flavonoids from chinese bayberry leaves induced apoptosis and g1 cell cycle arrest via erk pathway in ovarian cancer cells, Eur. J. Med. Chem. 147 (2018) 218-226.

[43] L. An, L.L. Han, Y.G. Zheng, X.N. Peng, Y.S. Xue, X.K. Gu, J. Sun, C.G. Yan,

Synthesis, x-ray crystal structure and anti-tumor activity of calix[n]arene polyhydroxyamine derivatives, Eur. J. Med. Chem. 123 (2016) 21-30.

[44] L.P. Lu, F.Z. Suo, Y.L. Feng, L.L. Song, Y. Li, Y.J. Li, K.T. Wang, Synthesis and biological evaluation of vanadium complexes as novel anti-tumor agents, Eur. J. Med. Chem. 176 (2019) 1-10.

[45] T.C. Chou, Drug combination studies and their synergy quantification using the chou-talalay method, Cancer Res. 70 (2010) 440-446.

[46] R. Florio, S. Veschi, V. di Giacomo, S. Pagotto, S. Carradori, F. Verginelli, R. Cirilli, A. Casulli, A. Grassadonia, N. Tinari, A. Cataldi, R. Amoroso, A. Cama, L. De Lellis, The benzimidazole-based anthelmintic parbendazole: A repurposed drug candidate that synergizes with gemcitabine in pancreatic cancer, Cancers (Basel). 11 (2019) 2042.

[47] M. Parra-Vargas, A. Sandoval-Rodriguez, R. Rodriguez-Echevarria, J.A. Dominguez-Rosales, A. Santos-Garcia, J. Armendariz-Borunda, Delphinidin ameliorates hepatic triglyceride accumulation in human hepg2 cells, but not in diet-induced obese mice, Nutrients. 10 (2018) 1060.

Journal Pre-proof

Journal Pre-proof

Highlights

1. Spiroketopyrazoles were synthesized as ACC inhibitors and antitumor agents.
2. **7j** and **7m** exhibited potent ACC inhibitory activity and antitumor activity.
3. **7m** induced cell cycle arrest and apoptosis in HepG2 cells.
4. Combination of **7m** with DOX synergistically decreased HepG2 cell viability.

Journal Pre-proof

Conflict of Interest Statements

The authors declared that they have no conflicts of interest to this work.

Journal Pre-proof